Acta Astronautica 226 (2025) 178–201

Contents lists available at ScienceDirect

Acta Astronautica

journal homepage: www.elsevier.com/locate/actaastro

VenSpec-H spectrometer on the ESA EnVision mission: Design, modeling, analysis

E. Neefs [a,*], A.C. Vandaele [a], R. De Cock [a], J. Erwin [a], S. Robert [a], I.R. Thomas [a], S. Berkenbosch [a], L. Jacobs [a], P. Bogaert [a], B. Beeckman [a], A. Brassine [a], N. Messios [a], E. De Donder [a], D. Bolsée [a], N. Pereira [a], P. Tackley [b], T. Gerya [b], S. Kögl [c], P. Kögl [c], H.-P. Gröbelbauer [d], F. Wirz [d], G. Székely [e], N. Eaton [f], E. Roibás-Millán [g], I. Torralbo [g], H. Rubio-Arnaldo [g], J.M. Alvarez [g], D. Navajas Ortega [g], L. De Vos [h], R. Sørensen [h], W. Moelans [h], A. Algoedt [h], M. Blau [h], D. Stam [i], E. Renotte [j], P. Klinkenberg [j], B. Borguet [j], S. Thomas [j], M. Vervaeke [k], H. Thienpont [k], J.M. Castro [l], J. Jimenez [l]

[a] Royal Belgian Institute for Space Aeronomy, BIRA-IASB, Ringlaan 3, 1180, Brussels, Belgium
[b] Eidgenössische Technische Hochschule (ETH) Zürich, Rämistrasse 101, 8092, Zürich, Switzerland
[c] KOEGL Space, Gruebacherstrasse 13, 8157, Dielsdorf, Switzerland
[d] Fachhochschule Nordwestschweiz (FHNW), Klosterzeigstrasse 2, 5210, Windisch, Switzerland
[e] Hochschule Luzern (HSLU), Technikumstrasse 21, 6048, Horw, Switzerland
[f] Space Acoustics, Peterwise, 3 8197, Rafz, Switzerland
[g] Instituto Universitario de Microgravedad "Ignacio Da Riva" (IDR/UPM), Universidad Politécnica de Madrid, 28040, Madrid, Spain
[h] OIP, Westerring 21, 9700, Oudenaarde, Belgium
[i] Leiden Observatory, Niels Bohrweg 2, 2333 CA, Leiden, the Netherlands
[j] AMOS, rue des Chasseurs Ardennais 2, 4031, Angleur, Belgium
[k] Brussels Photonics, Department of Applied Physics and Photonics (B-PHOT – TONA) and Flanders Make, Vrije Universiteit Brussel, Pleinlaan 2, 1050, Brussels, Belgium
[l] Instituto de Astrofisica de Andalucia, IAA-CSIC, Glorieta de la Astronomia, 18008, Granada, Spain

ARTICLE INFO

Keywords:
EnVision
Venus
Atmosphere
Space instrument
Spectrometer
Infrared
Nadir
Echelle grating
Filter wheel

ABSTRACT

VenSpec is a spectrometer suite on board ESA's EnVision mission to planet Venus, due for launch in November 2031. VenSpec consists of three spectrometers, VenSpec-M, VenSpec-U and VenSpec-H. VenSpec-H stands for **Ven**us **Spec**trometer with **H**igh resolution. It operates in the near-infrared wavelength range between 1.15 and 2.5 μm and it aims at mapping the near surface atmosphere during the night and the atmosphere above the cloud deck during the day. More specific, VenSpec-H will measure gases related to volcanism and surface changes on Venus. It will perform its measurements by means of nadir observations.

In this paper an overview is given of the main design requirements, followed by a description of the design activities performed during the feasibility study (phase A) and the preliminary definition (phase B1) of the instrument, including mathematical modeling and analysis, and prototyping. Focus is put on the optical working principle of the instrument, where an echelle grating, used as diffractive element, is combined with an inventive combination of filters for spectral band selection.

The design and development of VenSpec-H is done in a consortium under Belgian management and with important contributions from Belgian, Swiss, Spanish, and Dutch research institutes, universities, and industrial partners.

1. Introduction

SPICAV was an instrument on board ESA's Venus-Express mission. It contained three optical spectrometers one of which was the Belgian SOIR-channel (Solar Occultations in the Infrared), a compact high-resolution echelle grating spectrometer working in the infrared

* Corresponding author.
E-mail address: eddy.neefs@aeronomie.be (E. Neefs).

https://doi.org/10.1016/j.actaastro.2024.10.018
Received 21 January 2024; Received in revised form 13 July 2024; Accepted 7 October 2024
Available online 10 October 2024

domain between 2.3 and 4.3 μm [1]. SOIR has delivered a wealth of data on the chemical composition of the Venus atmosphere during the nearly ten years of intensive operation in space [2–4]. SOIR had an excellent instrument line profile (ILP) of 0.22 cm^{-1} FWHM over its complete wavelength range. This was achieved by a combination of an echelle grating and an acousto-optical tunable filter (AOTF). The AOTF served at pre-selecting orders from the incoming light prior to entering the spectrometer section. The fact that no moving parts were needed to scan through the targeted wavelength domain, made SOIR very appropriate for an interplanetary mission with limited resources [5–7].

Building on the success of SOIR on Venus-Express, ESA selected a successor of SOIR to fly on their ExoMars Trace Gas Orbiter mission. The instrument was called NOMAD (Nadir and Occultation for Mars Discovery) [8,9]. Unlike SOIR, that could only do solar occultation measurements, NOMAD was designed to also perform nadir measurements. To that purpose NOMAD was conceived as a double infrared spectrometer, with one channel (SO, standing for Solar Occultation) being a complete clone of SOIR, but with a second channel (LNO, standing for Limb, Nadir and Occultations) also allowing observations with fainter light sources like the Martian limb and the atmosphere at nadir. SO (2.3–4.3 μm - $\lambda/\Delta\lambda = 20'000$) and LNO (2.3–3.8 μm - $\lambda/\Delta\lambda = 10'000$) use the same optical concept as SOIR, an infrared echelle grating combined with an AOTF order sorter. NOMAD has sent back tens of millions of absorption spectra of the atmosphere of Mars and is still performing nominally today [10–12].

When ESA opened a call for ideas in April 2016 for a new planetary mission to Venus, it was logical to post again the candidature of a SOIR/NOMAD-like instrument. The goals for the EnVision mission, especially those related to the further study of the atmosphere, are more focused now than for Venus-Express. Amongst others, there is the idea to use the so-called night windows in the Venusian atmosphere to study very specific atmospheric compounds below the cloud deck. This resulted in an instrument proposal that strongly builds on the heritage of the LNO channel of NOMAD, but also has important differences. Only nadir observations are aimed at, and no longer in a broad spectral range, but in some very dedicated spectral bands. In that perspective VenSpec-H will resemble the VIRTIS instrument, also an echelle spectrometer operating in well-chosen narrow spectral bands, that flew on-board ESA's Venus-Express mission and successfully explored the atmosphere of Venus [13,14].

The VenSpec-H spectrometer is still based around an echelle grating but much more effort is put in reducing the thermal background of the instrument and to increase the SNR. Also, the idea of using an AOTF as order sorter is abandoned and replaced by another band selection method.

2. EnVision mission and VenSpec-H scientific goals

The EnVision mission was selected by ESA's Science Programme Committee on June 10th, 2021 as the fifth Medium-class mission in the Agency's Cosmic Vision plan and adopted for implementation on January 25th, 2024 after successful completion of phase B1.

The ambition of the EnVision mission is to provide a holistic view of Venus, its history, its activity, and its climate. It will do so by investigating the planet from its inner core to its upper atmosphere and to study any relevant interaction, e.g., between the surface and the atmosphere. To that purpose, the proposed scientific payload contains both spectrometers, to study the atmosphere and surface, and radars, to study the subsurface and planet interior [15,16].

The spectrometer suite selected for EnVision [17] consists of three completely independent channels, one called VenSpec-M (**m**ulti-spectral imager) under the responsibility of DLR (Germany) [18], one called VenSpec-U (**u**ltraviolet) under the responsibility of LATMOS (France) [19] and one called VenSpec-H (**h**igh resolution) under the responsibility of BIRA-IASB (Belgium) [20,21]. For the three channels, there is one central power supply and data handling unit (PSU/DHU) build under the responsibilities of DLR.

VenSpec-H will operate both at dayside and at nightside. During the night it will map the near-surface atmosphere (0–20 km) and the atmosphere below the clouds (20–45 km), while during the day it will look at the composition of the atmosphere above the cloud deck (65–80 km). Goal is to detect and map gases that play a role in volcanism and surface interactions. Four very specific narrow spectral bands are chosen for probing into the atmosphere. Band #2 is further split in band #2a and band #2b for reasons that will be explained later. Band #1, band #2 and band #3 allow to see through the cloud deck at night, they are the so-called spectral night windows of Venus. Table 1 gives an overview per band of the minimum required spectral range, the goal altitude range, and the targeted molecules. The science objectives of VenSpec-H and the full VenSpec suite are described in Ref. [15].

3. Design rules and requirements

3.1. General

The successes of SOIR and of the SO and LNO channels of NOMAD in observing the Venusian and Martian atmospheres, made it clear that also VenSpec-H must be based on the same optical principles. While SOIR and NOMAD-SO were solar occultation spectrometers, this technique is no longer applicable to VenSpec-H. The solar occultation technique does not allow to probe under the cloud deck. For that, nadir observations need to be performed, looking quasi-perpendicularly towards the planet at very specific wavelengths. The real precursor instrument of VenSpec-H therefore is NOMAD-LNO. EnVision will be a nadir-looking spacecraft, i.e., one of its decks will be completely dedicated to nadir-oriented instrumentation like VenSpec-H.

Below are described the most important design rules and requirements.

3.2. Orbital considerations

During the science phase of the mission, EnVision will orbit Venus in a circular orbit with a typical height of 390 km and a period of 5640 s. The X-axis of the S/C will be pointing towards and perpendicular to the surface of Venus. The VenSpec-H LoS is parallel to this axis.

VenSpec-H has a very elongated field-of-view (FoV) that is defined by the projection of one full detector column (or of the spectrometer slit) onto the Venusian disk. Hence, detector columns are spread along the spectral direction. To guarantee the required spectral resolving power during an observation, the instrument needs to be always oriented such that the velocity direction of the S/C is perpendicular to the long edge of the field-of view (Fig. 1).

During the mission, the S/C will flip several times over 180° to keep the cold face of the S/C as cool as possible. This does not hamper the

Table 1
Minimum required spectral range, altitude range, and targeted molecules.

	goal spectral band		altitude range	region	molecules
dayside	**band#2a**	2.34–2.42 μm	65–80 km	above clouds	H_2O, HDO, OCS, CO
	band#2b	2.45–2.48 μm			H_2O, HDO, OCS, SO_2, HF
	band#4	1.37–1.39 μm			H_2O, HDO
nightside	**band#1**	1.16–1.18 μm	0–15 km	below clouds	H_2O, HDO
	band#2a	2.34–2.42 μm	30–45 km		H_2O, HDO, OCS, CO
	band#2b	2.45–2.48 μm			H_2O, HDO, OCS, SO_2, HF
	band#3	1.72–1.75 μm	20–30 km		H_2O, HCl

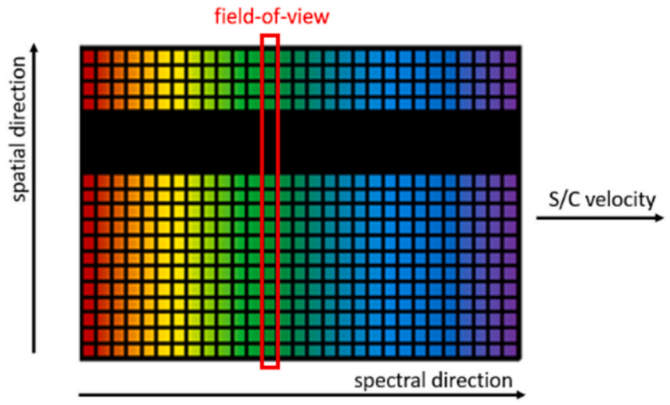

Fig. 1. Orientation of the detector and the instrument FoV with respect to the S/C velocity direction (spectral direction ≡ S/C Y-direction, spatial direction ≡ S/C Z-direction).

operation of VenSpec-H. The instrument can be operated both in N-S and S-N direction as long as the attitude is known on ground.

3.3. Alignment with S/C and other VenSpec instruments

During nightside observations, where the targeted height above the surface is 0 km, an across track footprint of 100 km is imposed. The same requirement of 100 km is imposed at dayside when measuring at an altitude of 60 km (the top of the cloud deck).

The along track footprint requirement during dayside measurements is set to 50 km but will rather be limited by the full well capacity of the detector. Depending on the spectral band, maximum integration times between 0.5 and 2 s will be used, corresponding to along track footprints of just a few km, considerably smaller than the required 50 km. During nightside observations, when the footprint is not limited by integration time, an along track footprint of 100 km is imposed. This footprint will then correspond to nightside integration times of approximately 15 s. From these (rather loose) spatial scales, a set of S/C pointing requirements (APE, RPE and AKE) is derived.

VenSpec-H has no very stringent co-alignment requirements between its LoS and the pointing axis of the S/C. It is imperative however to carefully register the misalignment between the two prior to launch (using instrument and S/C reference cubes), but also during flight (by looking at the Sun).

3.4. In-flight solar calibrations

Good knowledge of the exact viewing direction of VenSpec-H is important to interlink the measurements with the geographic location on the planet. To check the LoS misalignment with the S/C pointing axis, regular calibration measurements need to be performed using the Sun as a target. With Envision, solar calibration sessions are baselined with a repetition rate of 112 days. The solar calibration sessions will also be used to perform radiometric calibrations and straylight verification.

3.5. In-flight dark calibration

Besides regular solar calibrations, the VenSpec-H instrument requires dark calibrations during the mission, preferably also at a similar time interval as the solar calibrations. During a dark calibration session, the VenSpec-H LoS shall be pointed toward dark sky for 30 min, in a direction sufficiently away from the Sun and from Venus.

3.6. Signal-to-noise ratio (SNR)

Solar occultation instruments, like SOIR and NOMAD-SO, have the advantage of using the light of a bright source (the Sun prior to setting and just after rising). Achieving a good SNR is therefore simpler. This is not the case for nadir instruments, like NOMAD-LNO and VenSpec-H. The intensity of the entering light (the light reflected from the planet at day side and the proper emission of the planet at night side) is orders of magnitude lower than of direct sunlight even when attenuated by the atmosphere. Obtaining sufficient SNR therefore becomes one of the most challenging design drivers. Table 2 shows the purely science-based SNR requirements imposed in each of the spectral bands of VenSpec-H, and the derived requirements imposed to the optical designer (with 75 % margin). SNR requirements given in this table are for binned spectra, i.e., when all pixels in the spatial direction (a detector column) are co-added. These SNR values must be met in each spectral band for minimum radiance, taking into consideration all instrument sources of noise, and over the full lifetime of the mission.

SNR takes advantage of high incoming signal, but also of good noise suppression. One of the main drivers in near infrared nadir spectrometers is the suppression of thermal background, one of the main contributors to instrument noise. Therefore, it is decided that passive cooling of the spectrometer shall be implemented in Venspec-H.

3.7. Temperature management

To optimize SNR, it is of utmost importance that the infrared radiation of the optical elements in direct view of the detector array is minimized. In VenSpec-H all elements in the optical path, from the spectrometer slit onwards until the detector optics, will be cooled. They will be located together in a so-called cold (spectrometer) section, a box thermally isolated as much as possible from the rest of the instrument. This cold section will be refrigerated passively via a connection to a radiator at a (nearly permanent) cold face of the S/C. From an SNR perspective, a good working temperature setpoint is −60 °C, as can be seen in Fig. 2. At higher temperatures the SNR curve starts to drop off.

Having a cold section embedded in a warmer instrument gives rise to several challenges. The optical bench now is composed of a warm and a cold plate, that need to act as one. This composed bench needs to be thermo-elastically stable to guarantee the optical performance of the instrument over the duration of a science observation. Further, the heat exchange between the cold and the warm part of the instrument needs to be limited as much as possible.

It will be shown further that for optimal performance also the warm part of the instrument has specific thermal operational requirements. The working temperature range of the warm section is set to between −10 °C and 0 °C. For that, a connection will be made to a second, warmer S/C radiator.

As much as possible, heat producing elements have been detached from the optical bench. Obviously, not all power dissipators can be

Table 2
Binned SNR - science requirement per spectral band (w/o margin).

	required spectral band		SNR requirement	
			pure science (no margin)	towards designer (with margin)
dayside	**band#2a**	2.34–2.42 μm	≥100	≥175
	band#2b	2.45–2.48 μm		
	band#4	1.37–1.39 μm		
nightside	**band#1**	1.16–1.18 μm	≥48	≥84
	band#2a	2.34–2.42 μm	≥126	≥220
	band#2b	2.45–2.48 μm		
	band#3	1.72–1.75 μm	≥70	≥122

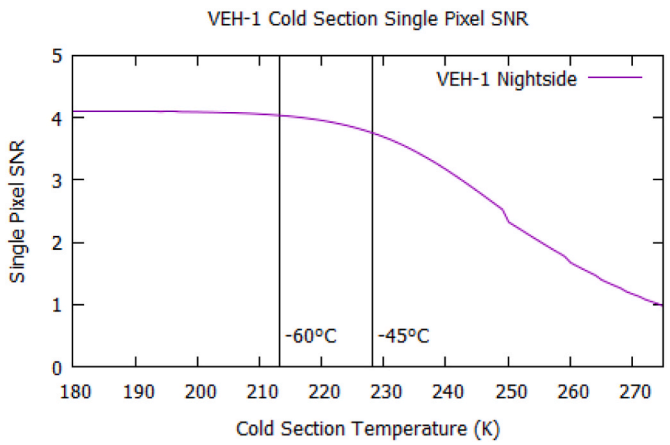

Fig. 2. Tendency plot for single-pixel SNR in band #1 (night side) as a function of cold section temperature (arbitrary SNR units).

removed (e.g., the detector). Still, VenSpec-H will have a separate electronic box, containing all electronic units that can operate at a distance from the bench.

Besides very specific operational temperature requirements, VenSpec-H must survive also in the non-operational environmental conditions imposed by the S/C. They are amongst others driven by the fact that the instrument is connected to radiators that potentially could also heat up the instrument or be colder than the nominal operational temperature. The qualification non-operational temperature is between −60 °C and +70 °C for the optical bench and between −50 °C and +60 °C for the electronic box.

3.8. Resolving power and requirements related to the instrument line profile (ILP)

To resolve sufficiently the absorption lines in the registered spectra, a resolving power $\lambda/\Delta\lambda$ of 7′000 is imposed across each of the spectral bands and homogeneous over the width of the detector. λ is the central wavelength of the spectral band and $\Delta\lambda$ is the FWHM of the spectral distribution seen by one pixel. This resolving power needs to be achieved for one pixel at dayside and for a full detector column at nightside. Also, a requirement is placed on the integral of the ILP (over a width equal to the number of pixels within $\Delta\lambda$). It shall be $\geq$ 69 % for band #1, band #2a and band #2b, and $\geq$53 % for band #3 and band #4.

Additionally, measures shall be taken in the design to avoid as much as possible the presence of ghost peaks and straylight. A requirement is imposed on out-of-field straylight during night observations, namely that in each spectral band, straylight coming from the Sun from an angle greater than 65° shall be below 0.1 % of the total signal. For in-field straylight a distinction is made between in-band straylight (shall be smaller than 2 % of the total signal) and out-of-band straylight (shall be smaller than 1 % of the incoming spectral radiance).

3.9. Image quality

VenSpec-H is not an imaging spectrometer and, hence, has no specific spatial resolution requirements, besides the earlier mentioned maximum footprint of 50 km × 100 km at dayside and 100 km × 100 km at nightside. The achievable footprint is defined by the position and velocity of the S/C and by the integration time of the detector. While during design care shall be taken to have the slit sharply imaged on the planet at one side, and on the detector at the other side, the main focus is to obtain good image quality in the spectral direction (perpendicular to the slit). Goal is to have the FWHM of the Line Spread Function (LSF) always smaller than the pixel pitch (24 μm).

During nightside observations it will be necessary to bin together all pixels in the spatial direction (full detector column). Hence, it is crucial that the image of the slit on the detector is as straight as possible, preferable contained within one pixel width (24 μm). Measures must be taken in the design to limit the curvature of the slit image (smiling). Tilting of the slit image on the detector shall also be minimized, e.g., by proper alignment of the detector.

3.10. Polarization

Sunlight that is scattered in the Venus atmosphere and reflected back is linearly polarized. The degree of polarization and the direction seen by VenSpec-H will depend strongly on the composition and the local properties of the atmosphere, on the illumination conditions and on the viewing configuration. Measuring the polarization adds significant value to the science capabilities of the instrument. Therefore, it is required that the VenSpec-H instrument has the possibility to perform polarization measurements in the dayside bands #2a, #2b and #4.

On the other hand, the fact that the incoming light during dayside observations will be polarized, will disturb the measurements during “normal” operation, at least if the instrument is sensitive to polarization. A scientific requirement is set out that restricts the allowable polarization sensitivity of the instrument to 1 %.

3.11. Summary of requirements

Table 3 summarizes the most important requirements of VenSpec-H. It must be clear that from these requirements the spectral performance (choice of bands, ILP, resolving power) and the detectability of the species (SNR) are the main drivers. Spatial resolution (footprint) can be relaxed if it helps reaching the main drivers. In the following chapters it will be shown that the SNR requirement is the most challenging.

4. Basic concepts

4.1. Diffraction

The preliminary design that was based on these requirements is described hereafter. Probably the earliest design decision was to stick to the heritage of the SOIR and NOMAD concept concerning the spectrometer itself, i.e., to use a high-dispersion echelle grating for light diffraction. Gratings have the distinct advantage over other types of spectrometers (based e.g., on cross-orthogonal dispersion) that the full height of the detector can be used to register spectral lines, allowing to improve the SNR by in-column binning. Disadvantage of a grating, at first glance, is that all orders appear superimposed at the output and, hence, on the detector. This can be solved by placing an order sorting device in front of the grating, limiting the light that reaches the grating to exactly one order.

4.2. Band selection

A study has been performed by Gooch and Housego (UK), the manufacturer of the SOIR and NOMAD AOTFs, to check the feasibility of an AOTF in the required spectral range (1.15–2.5 μm) and with the anticipated etendue of VenSpec-H. It appears that increasing the angle of incidence (orthogonal to the plane of diffraction) broadens the resolution. Increasing the aperture height of the AOTF reduces the required FoV again (for constant etendue) but at the expense of higher RF drive power, or lower diffraction efficiency (throughput) or both. It was concluded that with current technology it is very complicated to achieve an AOTF complying to the optical and power needs of VenSpec-H, without some significant compromises.

Unlike SOIR or NOMAD, VenSpec-H does not need to probe over a vast spectral range of some 200 spectral orders. In fact, it needs to look at only four spectral bands. Therefore, it was decided to use a filter wheel as spectral band selector in front of the grating instead of an AOTF. The

Table 3
Summary of VenSpec-H requirements.

Parameter	value or range					unit
	band #1	band #2a	band #2b	band #3	band #4	
wavelength λ	1.16–1.18	2.34–2.42	2.45–2.48	1.72–1.75	1.37–1.39	μm
SNR binned						
dayside		≥100	≥100		≥100	/
nightside	≥48	≥126	≥126	≥70		/
integral over ILP	≥69	≥69	≥69	≥53	≥53	%
Footprint						
across track						
dayside	≤100					km
nightside	≤100					km
along track						
dayside	≤50					km
nightside	≤100					km
resolving power λ/Δλ	≥7′000					/
polarization sensitivity	≤1					%

filter wheel will carry filters for band #1, band #2, band #3 and band #4.

Three of the bands (band #1, band #3 and band #4) correspond (more or less) to one grating order. Only band #2 is considerably larger than one order. For that reason, it has been decided to split band #2 in two parts, band #2a and band #2b. However, there is a strong science requirement to still be able to measure the complete band #2 (#2a + #2b) simultaneously. For splitting band #2 a detached filter pair is added further in the optical path, with two horizontal strips for band #2a and band #2b, one above the other. The light from band #2a travels through the top of the spectrometer, that of band #2b through the bottom, so that the two bands are simultaneously imaged in the top resp. bottom zone of the detector. The filter strips both have a good transmission for the wavelengths of bands #1, #3 and #4. They are both half passband with cut-off resp cut-on in the middle of band #2, as can be seen in Fig. 3.

The optical path is designed to have perfect correspondence between required spectral range and grating order for band #1. It will be shown later that for the other bands, still relatively good agreement can be found between minimum required spectral range and grating order.

4.3. Polarization

While it is scientifically interesting to analyze the polarization in the incoming light, it is, on the other hand, detrimental for its performance if the instrument is "oversensitive" to polarization. A polarization analysis of the preliminary optical design shows a sensitivity of maximum 8 % (at the edge of some of the spectral bands) (Fig. 4), significantly higher than the requirement (1 %). The logical solution would have been to add in the optical path a polarization scrambler to reduce the polarization sensitivity. This option has been thoroughly investigated but turned out not to be viable for programmatic reasons. It has been decided to adopt an alternative on-ground data processing solution for desensitizing the measurements to polarization.

The need to exploit the polarization content of the Venusian light had already led to the decision to include two polarization filters in the filter

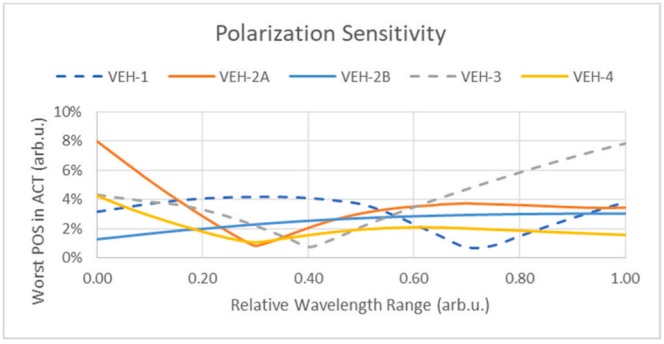

Fig. 4. Polarization sensitivity of the instrument in the different spectral bands.

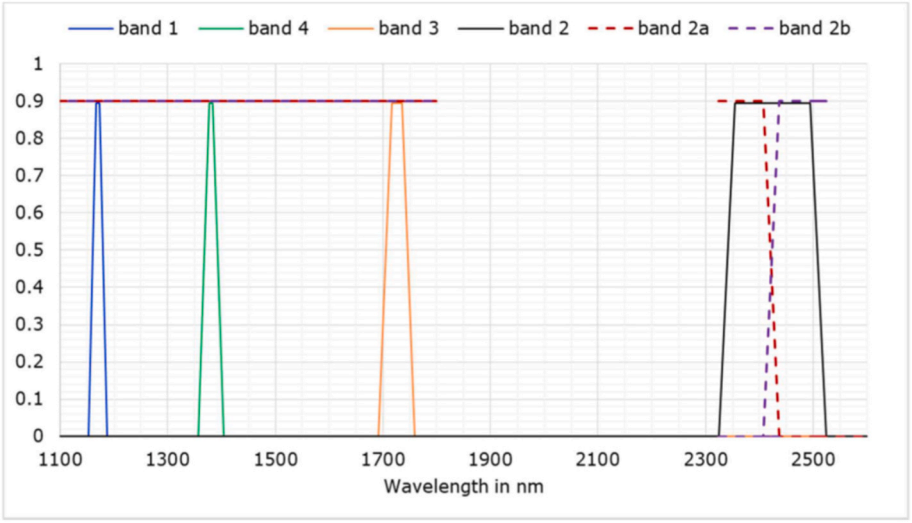

Fig. 3. Bands of the filters in the filter wheel (band #1, band #2, band #3 and band #4 – full lines) and the detached filter pair (band 2a and band 2b – dotted lines).

wheel, besides the four standard filters. The presence of these polarizers will allow to correct for the instrument's polarization sensitivity, by using them in an alternating measurement scheme with the standard filters during dayside measurements and consequent post-processing. This approach invalidates the earlier instrument polarization sensitivity requirement of 1 %. With the given instrument polarization sensitivity (Fig. 4) it is proven that the scientific goals can still be met.

5. Preliminary optical design

The optical path of VenSpec-H is designed by OIP Space Systems (Belgium). The optical principle is given in Fig. 5.

The figure shows three blocks: in orange the entrance section that is situated in the warm part of the instrument, in green the spectrometer section that corresponds to the cold part of the instrument, and in blue the detector section, again situated in the warm part of the instrument. Fig. 6 gives a more detailed overview of the different optical elements in the optical path.

The entrance section (#1 thru #3 in Fig. 6) consists of a window (#1 in Fig. 6) located in the rotatable door of the instrument (will be out of the optical path by the time science observations commence), followed by (one of the filters of) the filter wheel (#2 in Fig. 6), and the illumination optics (#3 in Fig. 6).

The filter wheel will be used to position one of the four standard filters in the optical path, corresponding to the four spectral bands of interest. To also analyze the polarization information in band #2 and band #4 at dayside, two wired grid polarizers will be included, leading to a total of six filters in the filter wheel. Also, an open and a closed position will be foreseen, hence, the filter wheel mechanism can be placed in eight distinct positions. The illumination optics (Fig. 7) is an objective consisting of a triplet of spherical lenses that focuses the incoming light beam onto the entrance slit of the spectrometer.

The first element in the spectrometer section is the filter-slit-assembly (#4 in Fig. 6) (Fig. 8). It contains the dual strip filter combination that splits band #2 in band #2a and #2b. The height of filter strips #2a and #2b is not equal. It is optimized to guarantee best binned SNR in the two bands (band #2a corresponds to 19, band #2b to 181 detector rows). On top of the horizontal strips the spectrometer entrance slit will be deposited, that defines the Field of View (FoV) of the spectrometer. The dimensions of the slit correspond to the full height of the detector and the width of one detector pixel. The slit will be made a bit longer to compensate for variations in the height of the focal plane, caused by temperature changes of the warm section. To compensate for the smile introduced by the grating, the slit will be curved so that the image of the slit is straight within one pixel. It is "closed" in the region where crosstalk between the filter strips is anticipated over a height corresponding to 88 detector pixels (so-called black zone). The filter-slit-assembly is placed in an intermediate image plane of the instrument to have the boundary between the horizontal filter strips sharply imaged on the detector.

The diverging light beam after the filter-slit-assembly is captured by an off-axis parabolic mirror (#6 in Fig. 6) (Fig. 9) that collimates the light again into a parallel beam and images the entrance pupil of the instrument on the grating. The parabolic mirror will be a monolithic element made from RSA 443. The surface where the mirror is located will be NiP-plated prior to manufacturing so that better surface quality is obtained. The back of the part will be hollowed to save mass.

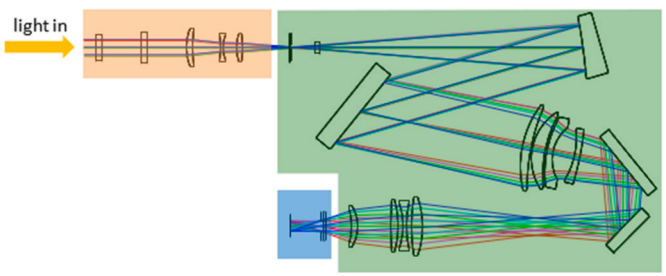

Fig. 5. Conceptual optical design of VenSpec-H.

Since the spectrometer slit is quite elongated, a compensation is needed for the aberration introduced by the parabolic mirror for field points at the long edges of the slit. To that end, a rectangular aspheric freeform corrector plate (Zernike polynomial) (#5 in Fig. 6) (Fig. 10) will be placed in front of the parabolic mirror 20 mm behind the filter-slit-assembly. The freeform corrector plate is manufactured by VUB's B-Phot Lab (Belgium). Filter-slit-assembly and freeform corrector plate will be mounted in a common mechanical holder (Fig. 10).

The central optical element in the spectrometer section is an echelle grating with periodic reflecting step (#7 in Fig. 6) (Fig. 11) that disperses the light into its spectral components. The grating will be a monolithic element built from RSA 443. A layer of NiP-plating will be applied on the optical surface before ruling so that a better surface roughness is obtained and, hence, better straylight performance. After ruling, a gold coating will be applied to the optical surface. Like the parabolic mirror, also the back of the grating will be hollowed to save mass. The VenSpec-H grating will be manufactured by AMOS (Belgium).

Fig. 12 shows some important grating parameters such as groove spacing and blaze angle at ambient temperature (to be used for manufacturing). During the optical design these parameters were tuned such that performance is optimized at the cold operational temperature.

The spectral bands of VenSpec-H correspond to grating orders 28, 29, 40, 50 and 59. Table 4 gives for each order the minimum and the maximum wavelength (1) as required, (2) as will be delivered by the grating, and (3) as will be seen by the detector. Also, the associated minimum and maximum diffraction angles are given.

The spectrally resolved light beam is imaged then on the detector. For that, two lens units are used, called the grating optics (#8 in Fig. 6) (Fig. 13) sitting right after the grating, and the detector optics (#11 in Fig. 6) (Fig. 14) located just in front of the spectrometer exit. Each group has four spherical lenses. Between the lens groups an intermediate image is formed. This is needed to image the entrance pupil on the cold shield of the detector.

Because the light beam needs to be returned towards the warm section at the front of the instrument, two folding mirrors (#9 and #10 in Fig. 6) are introduced between grating optics and detector optics. Like parabolic mirror and grating, they are monolithic parts made from RSA 443.

Just behind the exit point of the spectrometer section the detector section is situated. The detector (#13 in Fig. 6) is a focal plane array of 288 (spatial) by 384 (spectral) pixels cooled down to around 120 K. It sits in a vacuum dewar that is closed at the entrance by a dewar window (#12 in Fig. 6). To avoid that thermal background radiation from the warm enclosure perturbs the incoming signal, a conical cold shield is placed around the detector, equally cryocooled to 120 K, with just a small aperture at the front to let the light enter. This cold shield aperture (the exit pupil of the spectrometer) is the limiting aperture in the instrument and is imaged at two positions along the optical path: (1) at the filter wheel location (minimizes the size of the filters), and (2) on the grating (minimizes the size of the grating).

The spectral properties of the instrument (free spectral range, instrument line profile) are defined by the optical configuration and the characteristics of echelle grating, parabolic mirror, grating optics, and detector optics. To define the spectral sampling interval, also the pixel size of the detector (24 μm) must be considered.

Fig. 15 gives a comprehensive sketch of the operational concept of VenSpec-H, indicating the orientation of the detector and the filter-slit-assembly, the projection of the FoV on the surface of Venus, and the imaging on the focal plane array. The illumination optics define how sharply the slit is imaged on the surface of Venus and, hence, the spatial resolution in the direction perpendicular to the slit (S/C velocity direction). The spectrometer section defines how sharply the slit is imaged

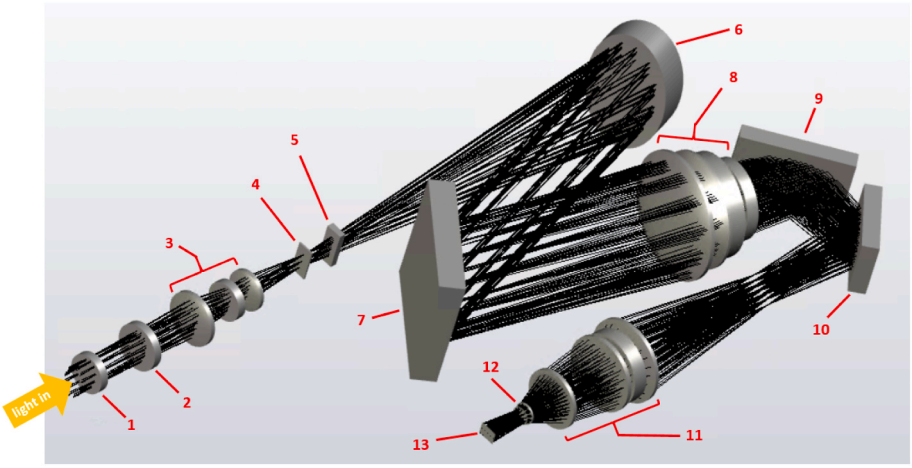

Fig. 6. Representation of the optical path of VenSpec-H.

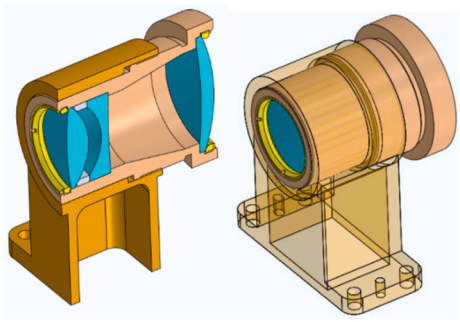

Fig. 7. Preliminary 3D assembly drawing of the illumination optics.

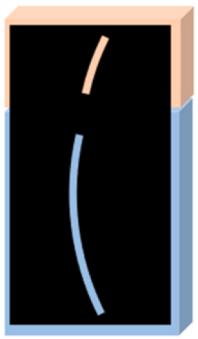

Fig. 8. The VenSpec-H filter-slit-assembly (curvature of slit exaggerated).

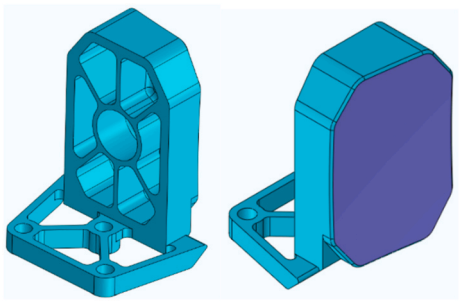

Fig. 9. Preliminary 3D drawing of the parabolic mirror.

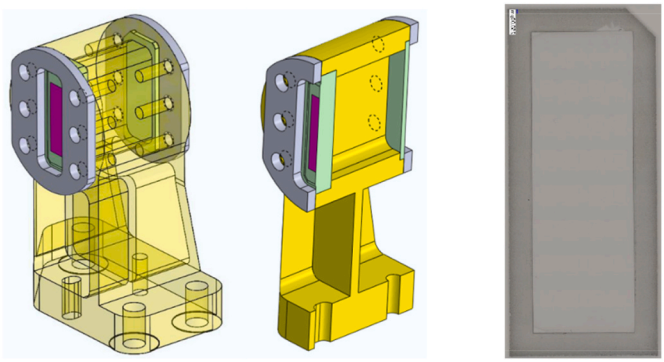

Fig. 10. Preliminary 3D drawing of filter-slit-assembly and freeform corrector plate in their holder (left) and real-scale FFCP prototype (right).

on the detector. The image of the slit together with the spectral sampling determines the spectral resolution. The combination of illumination optics plus spectrometer section defines how sharply the detector rows are imaged on the surface of Venus. This determines the spatial resolution in the direction parallel to the slit.

The focal lengths and magnifications of the different functional optical groups, both spatial and spectral, are summarized in Table 5. The overall F-number of the instrument is f/# = 3. The height of the optical axis above the horizontal plane of the cold base plate is 44 mm and 54 mm above the plane of the warm base plate.

6. Mechanisms design

6.1. Filter wheel mechanism

The filter wheel mechanism steers the filter wheel into one of eight uniformly distributed positions: six filter positions, one open position and one closed position (Fig. 16). The filters are mounted into the wheel using a clamp system that ensures well seating of the fused silica substrate filters and at the same time minimizes stresses. The wheel is held in place by a back-to-back dry lubricated bearing pair and is directly driven by a 1°-step stepper motor. To save dissipated energy, the motor will be driven in open loop to the next required filter in the shortest drive direction. A Hall sensor will be used for defining a reference position.

The assignment of the filters to the different positions in the wheel is a function of the expected science operations (e.g., nightside vs dayside). Considering the nominal duration of the mission and standard operational scenarios, the filter wheel mechanism will have to perform 1.4 million cycles (one cycle corresponding to a full 360° rotation).

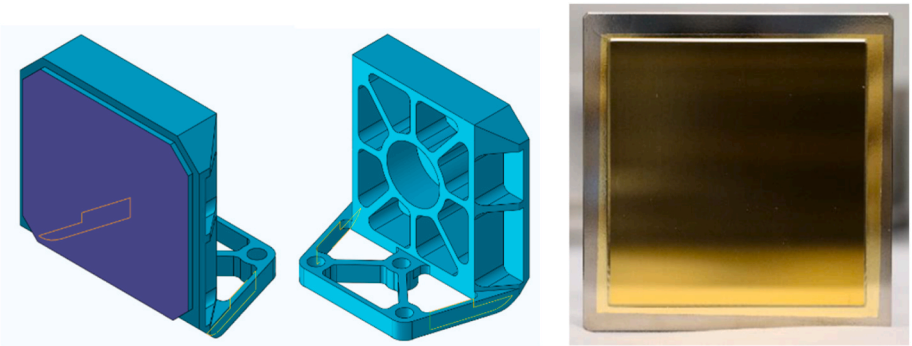

Fig. 11. Preliminary 3D drawing (left) and reduced-scale prototype (right) of the grating.

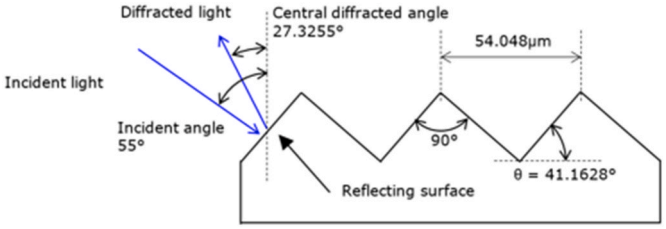

Fig. 12. Echelle grating configuration (at 20 °C).

Table 4
Minimum and maximum wavelength per grating order, as seen by the detector and the associated diffraction angles (at cold operational temperature).

parameter	value or range					unit
	band #1	band #2a	band #2b	band #3	band #4	
required wavelength range						
order	59	29	28	40	50	/
minimum wavelength	1.1600	2.3400	2.4500	1.7200	1.3700	µm
maximum wavelength	1.1800	2.4200	2.4800	1.7500	1.3900	µm
grating order						
minimum wavelength	1.1600	2.3398	2.4218	1.7043	1.3668	µm
maximum wavelength	1.1799	2.4218	2.5099	1.7474	1394.4	µm
range seen by the detector						
minimum wavelength	1.1492	2.3375	2.4209	1.6950	1.3561	µm
maximum wavelength	1.1903	2.4222	2.5087	1.7558	1.4045	µm
diffraction angle						
minimum diffraction angle	26.6350	25.9370	25.8880	26.3120	26.5120	°
maximum diffraction angle	28.0320	28.7810	28.8350	28.3740	28.1610	°

A load analysis has been performed with the proposed design of the ball bearings, taking into consideration operational and non-operational temperature ranges as well as the launch loads (quasi-static and random). With the selected preload on the bearing pair, no gapping is observed for the worst-case launch loads and the resulting Hertzian contact stress in the bearings on-orbit is in the range of 900–1′000 MPa. In these conditions the predicted life of the bearings is much higher than the needed 1.4 million cycles according to the Space Tribology Handbook [22] (Fig. 17). To increase confidence of the mechanism with the actual defined loads and temperatures, a detailed breadboard has been built that underwent a test campaign consisting of a vibration, a thermal-vacuum, a shock and a life test.

Design and development of the filter wheel mechanism is done by the Hochschule Luzern (Switzerland). The flight hardware will be built in Switzerland as well.

6.2. Shutter mechanism

To protect the instrument against atomic oxygen during the aerobraking phase of the mission, a one-shot turn window unit (also called shutter mechanism) is foreseen right behind the entrance aperture of the instrument inside the instrument cavity (Fig. 18). The shutter will be closed from launch until after aerobraking. Prior to the start of the science phase, it will be opened. Instead of a full aluminum lid, the shutter door has a transparent infrared grade fused silica window. This is a failsafe provision that will allow the instrument to perform nominally in case the door would not open, and to perform already at least one in-flight solar calibration before aerobraking.

The opening system is based on the thermal knife principle. The turn window is held by a polymer wire under spring tension. By applying electrical power to one of the thermal elements (nominal and redundant resistors) the wire will melt, and the mechanism rotates until it hits a hard stop, in a position where the window is no longer in the optical path. The spring force will keep the shutter in the open position. Like for the filter wheel, Hall sensors are used, here to detect the closed and open positions of the shutter and, hence, to verify if the actuation was successful.

Design and development of the shutter mechanism are done by DLR (Germany).

6.3. Integrated detector cooler assembly (IDCA)

The spectrometer slit will be projected on the sensitive area of the detector. It is crucial that the position of the detector is matched perfectly to the optics at the cold operational temperature, e.g., that the detector columns are nicely in line with the image of the spectral lines produced by the grating, or that the spectrometer image is not defocused. Placing the detector in the correct position with respect to the spectrometer will be subject of the optical alignment process (see further).

The 384 × 288 SWIR Mercury Cadmium Telluride (MCT) detector from AIM (Germany) will be used. It has an infrared focal plane array (FPA) to which a read-out multiplexer (ROIC) is hybridized using indium solder bump technology. The ROIC is described in a later section of this article. The MCT detector has the stoichiometric ratio of Cd to Hg adjusted to obtain the required cut-off wavelength. This photosensitive chip is backside illuminated. Therefore, the detector's CdZnTe substrate thickness is reduced to allow the photons to reach the sensing layer. A broadband SWIR anti-reflective coating is deposited on the MCT to reduce reflection losses from the entrance facet and to minimize ghost images from back-reflection. The FPA + ROIC hybrid is mounted on top

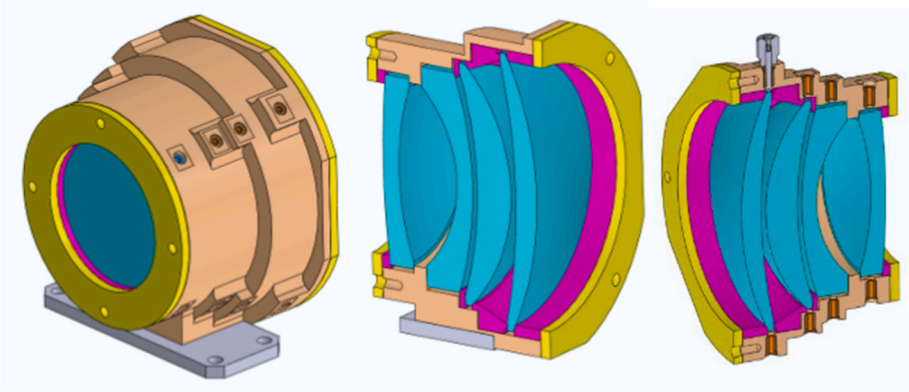

Fig. 13. Preliminary 3D drawing of grating optics in their holder.

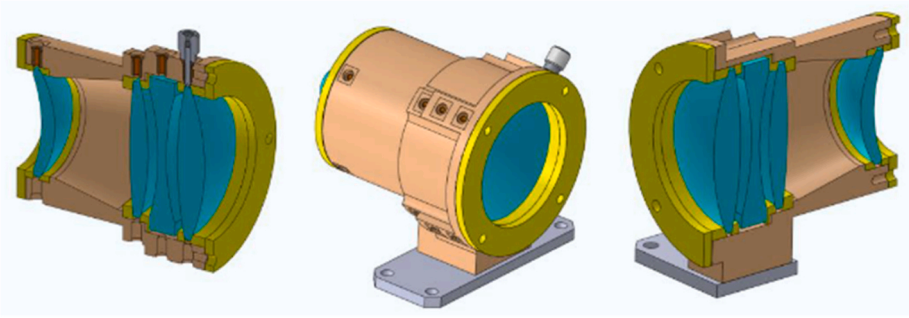

Fig. 14. Preliminary 3D drawing of detector optics in their holder.

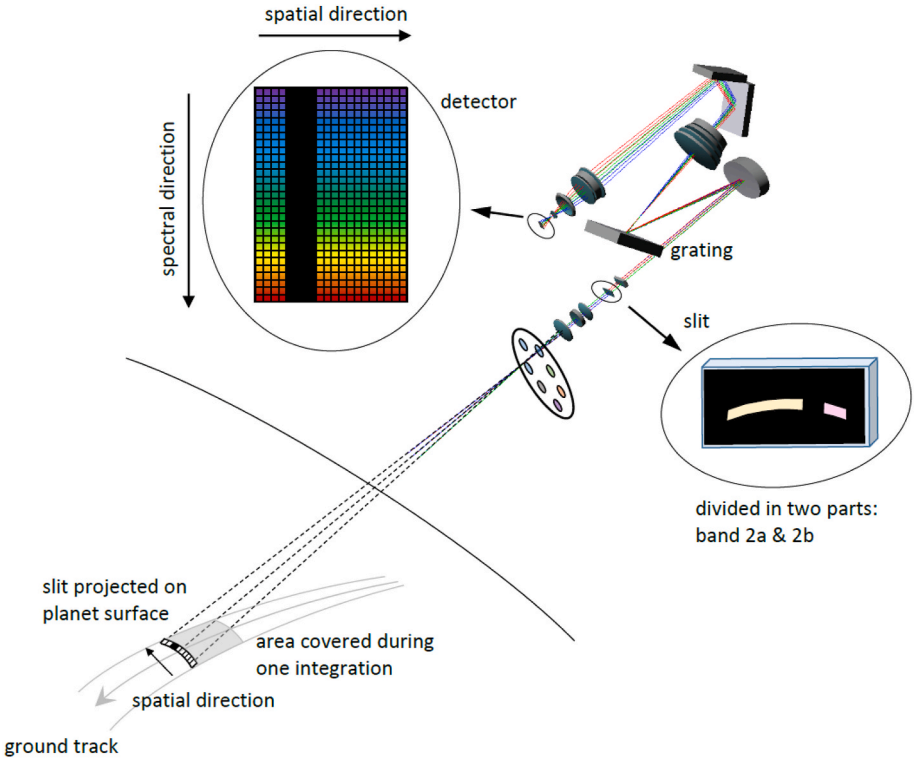

Fig. 15. Sketch of the VenSpec-H operational principle.

of a ceramic substrate.

The dewar entrance window is made of sapphire to be compliant with the required spectral bandwidth. Fig. 19 gives a sketch of the stack-up of the detector and ROIC. The dark current of the detector, important for the calculation of the overall instrument SNR, is specified to be 0.23 nA/cm^2 at beginning and 0.83 nA/cm^2 at end of life. The quantum

Table 5
First order optical properties.

optical module ↓	focal length or magnification			f/#		
	spatial	spectral	unit	spatial	spectral	unit
full instrument	60.0	38.7	mm	3	3	/
illumination optics	81.7	81.7	mm	4.08	6.32	/
spectrometer optics	0.735 ×	0.474 ×	/	3	3	/
parabolic mirror	245.0	245.0	mm	4.08	6.32	/
Grating	1.000 ×	0.646 ×	/	–	–	/
grating/detector optics	180.0	180.0	mm	3	3	/

efficiency of the detector is at least 72 % over the applicable wavelength range. More details about this IDCA can be found in Ref. [23].

The FPA is cooled with an SF070 Stirling linear cryocooler compressor. This cooler has an expected mean lifetime of more than 20′000 h, largely sufficient to cover the nominal EnVision mission and even potential extensions.

7. Thermal background, signal and noise

7.1. General

The SNR is a measure for the sensitivity of an instrument. When performing nadir observations, the incoming signal is weak and, hence, suppression of the instrument's noise is important. Many parameters influence the SNR, acting either on the portion of incoming signal that reaches the detector or on the noise. During VenSpec-H operation from each "signal + background" spectrum, a "background-only" spectrum, taken in the same conditions, will be subtracted, either on-board or on-ground. Taking the noise contributions from the background spectrum into account, the SNR for N binned pixels is calculated by Equations (1) and (2).

$$SNR = \sqrt{N}.\frac{S.\tau}{\sqrt{([1+SLF].S + 2.DC + 2.TB).\tau + 2.RO^2 + 2.ADC^2}} \quad \text{(Equation 1)}$$

with

$$ADC = \frac{FWC}{\sqrt{12}.2^{bit}} \quad \text{(Equation 2)}$$

Here S is the signal on one detector pixel, τ the integration time, SLF the straylight fraction, DC the dark current of the detector, TB the thermal background, RO the read-out noise, ADC the analog-to-digital conversion noise, FWC the full well capacity of the detector, and bit the number of bits (14) of the analog-to-digital converter.

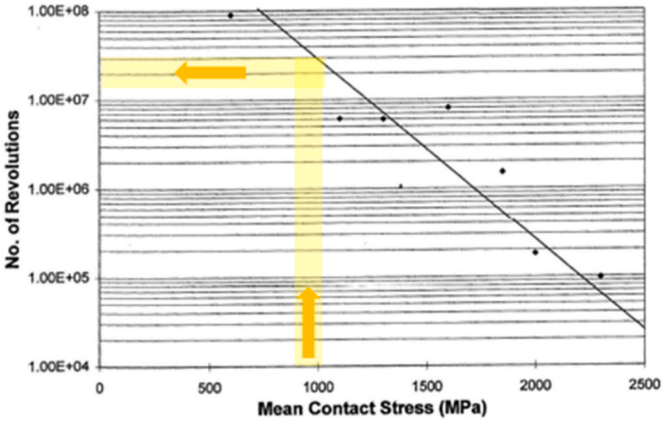

Fig. 17. Achievable number of revolutions as a function of mean contract stress [20].

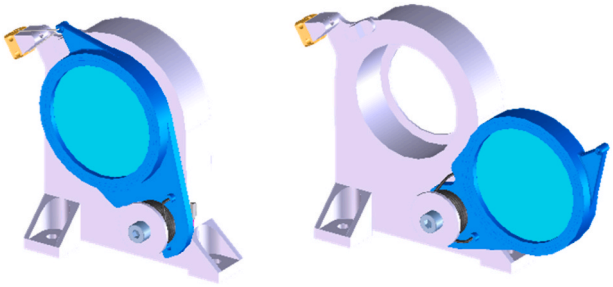

Fig. 18. 3D drawing of the shutter mechanism (left in closed position, right in opened position).

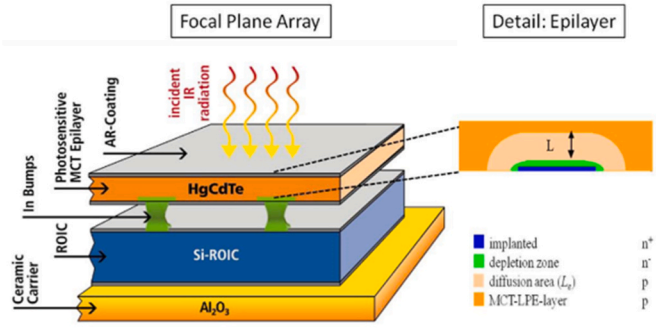

Fig. 19. *Focal Plane Array and ROIC stack-up (courtesy AIM).*

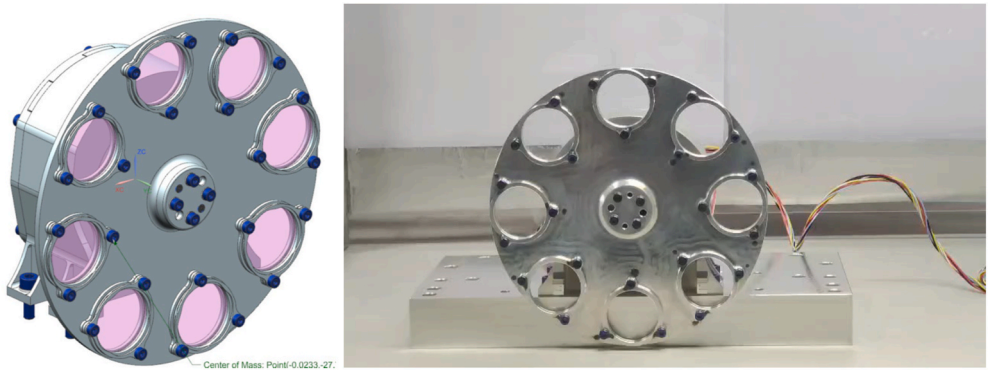

Fig. 16. Design drawing (left) and prototype (right) of the VenSpec-H filter wheel mechanism.

The integration time τ will be limited by either of the following parameters (Equation (4)), whichever is smallest: (1) the time for which the maximum total signal (S_{max}) in the wavelength band reaches 85 % of the full well capacity (FWC) of the detector, or (2) the time for which the ground distance traveled by the S/C reaches the maximum allowed target sampling distance.

$$\tau \leq \frac{85\%.FWC}{S_{max}+DC+TB} \quad \text{or} \quad \tau \leq \frac{SD}{R+T}\sqrt{\frac{(R+H)^3}{G.M}} \qquad \text{(Equation 3)}$$

Here SD is the maximum allowed sampling distance, R the radius of Venus, T the highest target altitude of interest (cloud tops at 60 km during dayside, and surface at 0 km during nightside), H the flight altitude of the S/C, G the gravitational constant, and M the mass of Venus.

For dayside observations the VenSpec-H measurement is full well limited (left in Equation (3)). For night side observations the integration time is limited by the required footprint (right in Equation (3)).

7.2. Signal

The incoming signal S during a nadir observation can be calculated from the spectral radiance L (Table 6) at the entrance of the instrument and the transmission function of the instrument, with Equation (4).

$$S(L) = L.\frac{\lambda}{h.c}.T(\lambda).QE(\lambda).p^2.2\pi.\left(1-\sqrt{1-\frac{1}{4.F^2}}\right).\frac{\lambda}{R} \qquad \text{(Equation 4)}$$

Here λ is the wavelength, T the transmission of the instrument from entrance to detector, QE the quantum efficiency of the detector, p the pixel pitch, F the F-number defined by the cold shield inside the detector dewar, and R the resolving power of the instrument. Good matching between the F-numbers of the optics and the detector (see Table 5) improves the SNR. The signal is also influenced by the grating transmission. The grating's diffraction efficiency varies over wavelength and hence is different in each band. Due to the dispersion inside one order, diffraction efficiency also varies from pixel to pixel.

7.3. Noise

The most important source of noise is the (temperature dependent) thermal background. Cooling down the optical and mechanical elements that are inside the FoV of the detector improves the SNR. Therefore, Venspec-H will have a cooled spectrometer section that was initially foreseen to operate at −60 °C. Cooling will be done passively, by means of a radiator at a cold face of the S/C. Early assessment by ESA has shown that it would be technically challenging to guarantee a temperature of −60 °C in the orbital configuration around Venus as designed for this mission. Therefore, a compromise has been reached to cool the spectrometer section down to −45 °C (see Fig. 2).

Optical and mechanical elements that are viewed by a pixel (even partly) contribute to the thermal background received on that pixel. The thermal background TB can be calculated with the Planck black-body emission of the element, its emissivity and transmission, and its etendue as viewed from the pixel, with Equation (5).

$$TB(\varepsilon,T) = \varepsilon.p^2.\Omega.\int_0^\infty \frac{2.c}{\lambda^4}.\frac{1}{exp\left(\frac{h.c}{k.T.\lambda}\right)-1}.T_{TB}(\lambda).QE(\lambda).d\lambda \qquad \text{(Equation 5)}$$

Here ε is the emissivity of the surface, T the temperature of the surface, λ the wavelength, p the pixel pitch, Ω the solid angle of the surface as seen by the pixel, T_{TB} the transmission of the optics from the emitting surface to the detector, and QE the quantum efficiency of the detector.

Elements in front of the filter wheel are contributing only marginally to the thermal background, because the filters limit the light traveling to the detector to just a small passband. Emitted thermal background of elements in front of the slit is diffracted by the grating, but background from all the grating orders will pile up on a pixel. For elements behind the spectrometer slit (slit included) the full thermal background (i.e., all wavelengths) will be seen by a pixel.

Also, not all the elements contributing to the thermal background are at the same temperature. Parts inside the detector dewar (e.g., the cold shield) will be at 120 K, the spectrometer optics (e.g., grating, parabolic mirror, etc.) will be at −45 °C, the illumination section in front of the slit and the detector dewar window will be at approximately 0 °C.

From the denominator of Equation (1) it is seen that the noise is the sum of several contributions: the shot noise (coming from the signal S), the dark current noise (coming from the dark current DC), the Johnston noise (coming from the thermal background TB), the read-out noise from the electronics, and the analog-to-digital conversion noise.

Table 7 shows the maximum integration times for each band and the corresponding SNR considering end-of-life conditions (assumptions as known at end of phase B1). For nightside observations SNR is very low. Therefore, it will be necessary to bin pixels together to throttle up the SNR (by binning N pixels the SNR is multiplied by $\sqrt{N}$). This is shown in the last column of Table 7. That column shall be compared to the requirements for binned SNR from Table 2. For nightside observations the requirement is not met in band #1. Still the value is deemed to be sufficient to achieve the science goals.

8. Optical performance and quality

8.1. Quality of the slit image on the detector

It is true that illumination optics plus spectrometer section together define how sharply the detector rows are imaged on Venus, i.e., the spatial resolution (parallel to the slit). But since there are no stringent requirements on spatial resolution for VenSpec-H (besides some lose

Table 7
Expected SNR at end-of-life per spectral band.
(band #1, #3, #4 binning over 288 pixels –band #2a binning over 19 pixels, band #2b binning over 181 pixels).

	spectral band		integration time		binned SNR
			value	unit	
dayside	band#2a	2.34–2.42 μm	1.23	s	11′831
	band#2b	2.45–2.48 μm			9′419
	band#4	1.37–1.39 μm	0.46	s	29′596
nightside	band#1	1.16–1.18 μm	14.29	s	53
	band#2a	2.34–2.42 μm	14.29	s	220
	band#2b	2.45–2.48 μm			169
	band#3	1.72–1.75 μm	14.29	s	672

Table 6
Spectral radiance (L) at reference wavelengths in each band for dayside and nightside.

	band #1	band #2a	band #2b	band #3	band #4	unit
reference wavelength	1.170	2.380	2.460	1.730	1.380	μm
dayside spectral radiance	–	$1.58.10^{+1}$	$1.1\&0.10^{+1}$	–	$1.44.10^{+2}$	W/m2/sr/μm
nightside spectral radiance	$1.87.10^{-2}$	$6.37.10^{-2}$	$1.37.10^{-2}$	$1.13.10^{-1}$	–	W/m2/sr/μm

footprint requirements), focus is put entirely on the image quality in the spectral direction (perpendicular to the slit). A good measure for that "spectral" image quality is the line spread function (LSF). Table 8 gives the predicted FWHM of the LSF for some rows on the detector and for one wavelength in the middle of each spectral band. The LSF is always smaller than the pixel pitch (24 μm).

8.2. Smile

The straightness of the image of the slit on the detector is given by the smile of the spectrometer. Above, it is already explained that the spectrometer slit is curved to compensate for the smile effect of the spectrometer. In Table 9 the predicted residual smile is given for some rows on the detector and for one wavelength in each spectral band. The smile is the difference in spectral position of a field point with respect to the average spectral position over the slit. Smile is worse at the edges of the detector. Another effect is tilt of the slit image on the detector, but this can be compensated for by proper alignment of the detector during the assembly process of the instrument.

8.3. Instrument line profile

The instrument line profile (ILP) is defined as the intensity profile of the slit image when illuminated by monochromatic light and is calculated by convoluting the LSF with a top hat function equal to the width W of the geometrical image of the slit (Equation (6)).

$$ILP\ (\lambda) = \int LSF(\lambda - x).\prod\left(\frac{x}{W}\right).dx \qquad \text{(Equation 6)}$$

Table 10 gives the predicted FWHM of the ILP for some rows on the detector and for one wavelength in each spectral band, and for the case where a complete detector column is binned (full slit). Table 11 gives the fraction of the total energy of the ILP that falls within the FWHM.

8.4. Resolving power

The resolving power R is the spectral response of a pixel at a given wavelength λ and is written as λ/Δλ, where Δλ is the wavelength band seen by that pixel. Δλ is calculated from the pixel size p, the spectral sampling interval (SSI) and the FWHM of the spectral response function (SRF) (Equation (7)).

$$\Delta\lambda = \frac{FWHM_{SRF(\lambda)}}{p}.SSI(\lambda) \qquad \text{(Equation 7)}$$

The SSI is wavelength dependent. Averaged over the full slit height, it is around 0.11 nm/pix in band #1, 0.22 nm/pix in band #2a, 0.23 nm/pix in band #2b, 0.16 nm/pix in band #3, and 0.13 nm/pix in band #4. To calculate the SRF of a pixel, the convolution shall be done of the ILP and a top hat function with a width equal to the pixel size p (Equation (8)).

$$SRF(\lambda) = \int ILP(\lambda - x).\prod\left(\frac{x}{p}\right).dx \qquad \text{(Equation 8)}$$

Table 12 gives the predicted resolving power for some rows on the detector and for one wavelength in each spectral band, and for the case where a complete detector column is binned (full slit). A nominal resolving power of at least 8′500 is achieved in all cases, well above the required 7′000. The variation over a spectral band is not larger than 8 %.

8.5. Out-of-field straylight

As in any optical instrument, the correct functioning of VenSpec-H can be perturbed by light from other sources entering unwantedly in the instrument's FoV during nominal operation (e.g., direct sunlight or any light scattered from the S/C body). When this light succeeds in entering the spectrometer section within the solid angle seen by the detector, it will degrade the performance of the instrument. While it is not possible to have a perfect exclusion of this out-of-field straylight, measures can be taken to constrain it as much as possible (e.g., adding intermediate apertures or an entrance baffle).

Fig. 20 (left) shows the simulated radiance in angle space and the normalized cross-section in the along-track direction. Broadly imaged straylight from the lens surfaces extends to approximately 10° away from the LoS in the along-track direction but is more than four orders of magnitude less intense than the peak. This will be constraint to 5° by adding apertures (1 mm wider than the beam size) at the entrance aperture, in front of the filter wheel and in front of the illumination optics.

Also, sharply imaged peaks are seen around the main peak, due to non-parallel surfaces in the optical path. Fig. 20 (right) proves that by tilting the filter wheel mechanism over 5° in the perpendicular direction, some of these sharp ghosts (those originating between filter and slit) disappear. Remaining out-of-field straylight signatures can most probably be cancelled out by including also a short external baffle at the entrance of the instrument and by putting tight tolerances on the tilt and wedge of the different flat optical surfaces inside. An in-depth straylight analysis still needs to be performed in phase B2.

8.6. In-field straylight

Light reflection between reflective surfaces (ghosts), degraded surface quality of the optical surfaces, light reflecting back from the detector surface, light reflected at the wrong angle from the grating, and contamination can cause unwanted images or straylight on the VenSpec-H detector. Manufacturing the optical elements with high tolerance, with good surface properties (e.g., surface roughness) and/or applying proper anti-reflective coatings helps reducing ghosting effects, as well as proper particulate contamination management.

Fig. 21 shows the results from a preliminary straylight simulation for the wavelength where ghosting effects are worst (1.17 μm in band #1). Three different micro-roughness RMS values were simulated for the refractive elements (lenses), while the roughness of the reflective surfaces (grating and mirrors) with NIP plating layer was constant at a value slightly above 4 nm RMS. The red horizontal line indicates the requirement level for the maximum allowed (unwanted) in-field in-band straylight (≤2 % of the total signal). It can be seen from these preliminary results that surface roughness of the refractive elements needs to be better than 5 nm RMS, which is achievable by polishing the lenses properly. However, the effects of the adjacent orders (out-of-band) still need to be thoroughly examined.

Table 8
FWHM of the LSF for some rows on the detector and one wavelength per spectral band.

band	wavelength	row 1	row 45	row 68	row 101	row 188	row 217	row 255	row 288	unit
band#1	1.170	5.5	5.5	5.8	6.3	6.3	5.8	5.5	5.5	μm
band#2a	2.380	–	–	–	–	8.3	8.1	7.9	8.0	μm
band#2b	2.465	9.1	8.6	8.6	8.7	–	–	–	–	μm
band#3	1.734	5.9	6.1	7.3	8.9	8.9	7.3	6.1	5.9	μm
band#4	1.381	13.2	9.2	9.0	8.4	8.4	9.0	9.2	13.2	μm

Table 9
Smile for some rows on the detector and one wavelength per spectral band.

band	wavelength	row 1	row 45	row 68	row 101	row 188	row 217	row 255	row 288	unit
band#1	1.170	0.9	−0.3	−0.4	−0.1	−0.1	−0.4	−0.3	0.9	µm
band#2a	2.380	–	–	–	–	−0.7	−0.7	−0.7	−0.7	µm
band#2b	2.465	1.7	−0.1	−0.8	−0.8	–	–	–	–	µm
band#3	1.734	1.7	−0.1	−0.8	−0.8	−0.8	−0.8	−0.1	1.7	µm
band#4	1.381	1.0	−0.3	−0.5	−0.2	−0.2	−0.5	−0.3	1.0	µm

Table 10
FWHM of the ILP for some rows on the detector and one wavelength per spectral band.

band	wavelength	row 1	row 45	row 68	row 101	row 188	row 217	row 255	row 288	slit	unit
band#1	1.170	24.7	24.7	24.8	24.9	24.9	24.8	24.7	24.7	24.8	µm
band#2a	2.380	–	–	–	–	24.9	24.8	24.7	24.8	24.9	µm
band#2b	2.465	25.3	25.0	25.0	24.9	–	–	–	–		µm
band#3	1.734	24.8	24.8	25.1	25.3	25.3	25.1	24.8	24.8	24.9	µm
band#4	1.381	25.3	25.1	24.9	24.9	24.9	24.9	25.1	25.3	25.1	µm

Table 11
Fraction of total energy of ILP in FWHM for some rows on the detector and one wavelength per spectral band.

band	wavelength	row 1	row 45	row 68	row 101	row 188	row 217	row 255	row 288	slit	unit
band#1	1.170	85.4	85.4	84.2	83.4	83.4	84.2	85.4	85.4	84.3	%
band#2a	2.380	–	–	–	–	81.3	81.8	82.2	81.3	81.1	%
band#2b	2.465	78.5	80.0	80.4	80.5	–	–	–	–		%
band#3	1.734	85.0	84.2	81.8	80.2	80.2	81.8	84.2	85.0	82.2	%
band#4	1.381	79.2	81.4	82.2	82.6	82.6	82.2	81.4	79.2	81.2	%

Table 12
Resolving power for some rows on the detector and one wavelength per spectral band.

band	wavelength	row 1	row 45	row 68	row 101	row 188	row 217	row 255	row 288	slit	unit
band#1	1.170	9′490	9′494	9′364	9′261	9′261	9′364	9′494	9′490	9′383	/
band#2a	2.380	–	–	–	–	9′071	9′147	9′217	9′139	9′068	/
band#2b	2.465	8′794	8′994	9′039	9′054	–	–	–	–		/
band#3	1.734	9′580	9′490	9′185	9′033	9′033	9′185	9′490	9′580	9′274	/
band#4	1.381	8′846	9′066	9′167	9′221	9′221	9′167	9′066	8′846	9′045	/

9. Key instrument parameters

Sizing of space instrumentation is often driven by dimensional and mass considerations. An acceptable compromise with scientific performance needs to be found. In the case of VenSpec-H, SNR, footprint, polarization and resolving power requirements are the main scientific drivers. With the presented design most of these science drivers are met, sometimes only marginally, while keeping the size and mass of the instrument within the limitations.

Table 13 gives an overview of the key parameters of the VenSpec-H instrument. Note that ESA has allocated a total mass to VenSpec-H of 22′546 g. The design mass of the instrument including applicable maturity and system margins at this time in the development process overruns this allocation slightly. The mass of the instrument excluding margins is 18′872 g though (14′476 g for optical bench, 3′796 g for electronic box), well below the allocation.

10. Mechanical structure, structural analysis, and alignment

10.1. Mechanical structure

VenSpec-H will have two mechanical units, the optical bench and the electronic box (Fig. 22). The optical bench structure consists of a warm base plate (Al 6061-T6), a warm cover, a cold base plate (Al 6061-T6) that is mounted into a shallow cavity on the warm base plate, and a cold cover. The warm and cold base plates carry all the optical elements.

The warm base plate will be mounted by means of four titanium (Ti6Al4) bi-pod feet to the S/C (Fig. 23 left) providing thermal and mechanical decoupling from the S/C deck. Although four (and not three) feet are used, they give sufficient elasticity to act together as a quasi-isostatic mount of the instrument. The cold base plate will be mounted on the warm base plate by means of four glass fiber reinforced plastic (GRFP) blades with aluminum end fittings at both sides (Fig. 23 right), oriented all towards the invariant point (fixed pin) of the cold base plate. This fixed pin has a Ti6Al4 kernel inside a GRFP body. These five elements will have very low thermal conductivity.

The covers that are placed over the cold and warm sections will be made from sandwich panels with aluminum face sheets and honeycomb cores. Some of the more complex covers (e.g., front covers of cold and warm section, rear cover of warm section) will be machined aluminum plates.

The electronic box of the VenSpec-H instrument is a self-standing unit, detached from the optical bench, with a dedicated mechanical enclosure (Al7075-T7351) consisting of four individual frames each lodging one electronic board (Fig. 24).

Most of the mechanical elements, and especially those close to the optical path, will undergo a space qualified optically black anodization that limits scattering of light and keeps thermal background as low as possible. Contact surfaces between mechanical parts will be free of anodization but treated with Surtec 650 for good electrical conductivity.

10.2. Structural model and analysis

Based on the CAD model of the instrument, a finite element

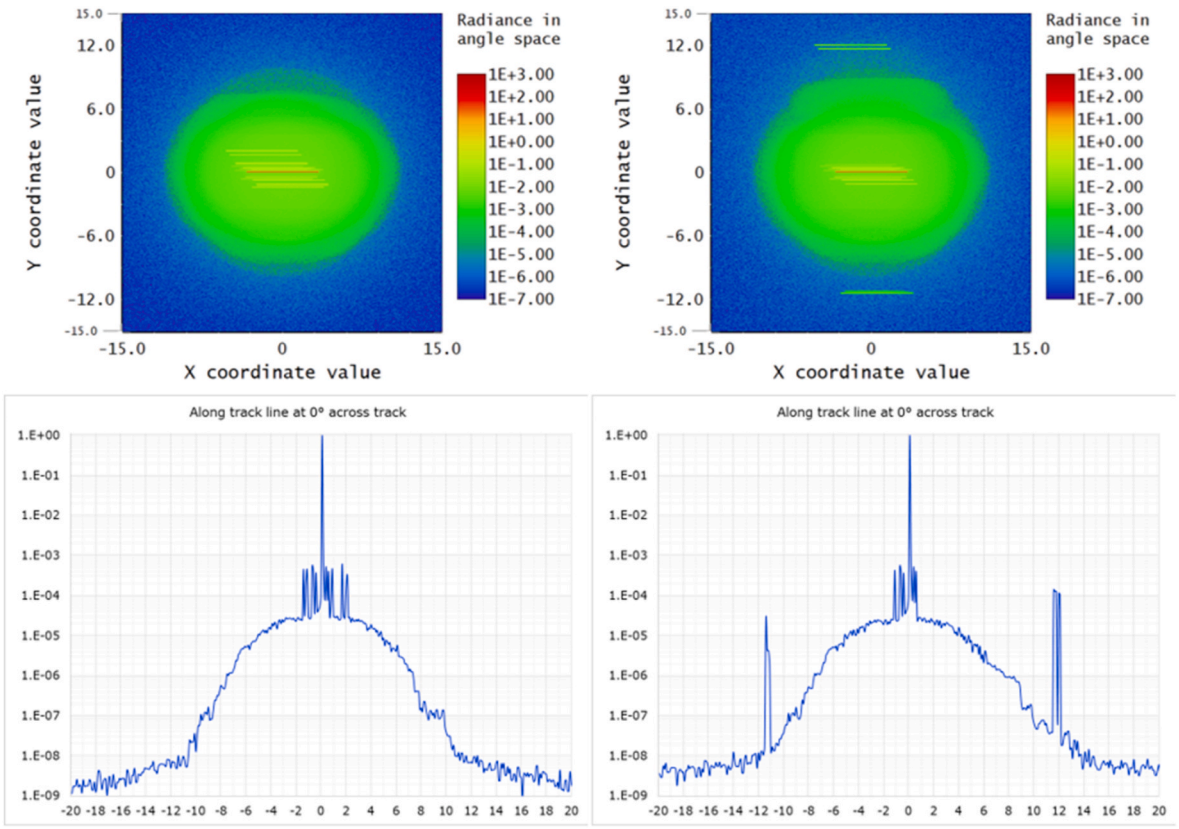

Fig. 20. Radiance in angle space (top) and along track normalized cross section (bottom) with random wedge and tilt of the filter and shutter window. Left: with filter wheel perpendicular to optical axis. Right: with filter wheel at 5° angle.

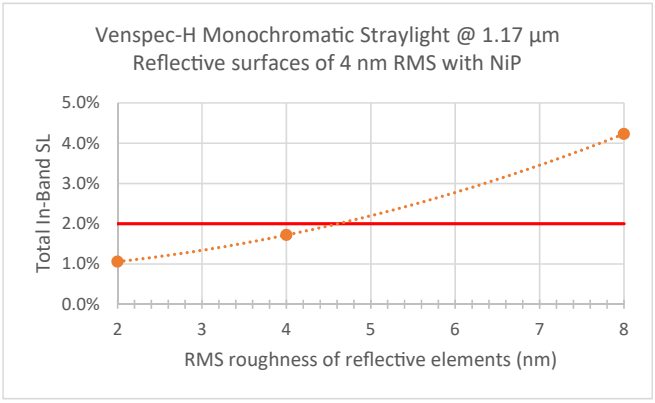

Fig. 21. In-field in-band straylight simulation including ghosting effects for band #1 at 1.17 µm.

Table 13
Summary of key instrument parameters.

parameter	value	unit
FoV	6.68 × 0.13	° x °
entrance aperture shape	circular	–
entrance aperture diameter	40 mm	mm
mass (without margins)		
optical bench	14′476	g
electronic box	3′796	g
dimensions (no harness)		
optical bench	632.0 × 407.1 x 264.0	mm x mm x mm
electronic box	211.5 × 241.5 x 129.8	mm x mm x mm
operational temperature		
cold section	−45	°C
warm section	0 – +10	°C
detector	120	K

mathematical model (FEM) was built in NASTRAN, both for the optical bench and the electronic box (Fig. 25 left and Fig. 26 left). The FEM of the optical bench has approximately 232′000 nodes, that of the electronic box 118′000. From these FEMs also reduced models are derived for insertion in the S/C structural model.

With the FEMs the stiffness of the two units has been verified by normal mode analysis. Eigenfrequencies and the associated modal effective masses (MEM) for the 3 translational and the 3 rotational degrees of freedom are calculated up to 2 kHz. The first three eigenmodes of the optical bench are the fundamental modes in X-, Z- and Y-direction at frequencies of 178 Hz, 187 Hz and 205 Hz respectively, well above the required 140 Hz (Fig. 25 right). For the electronic box, the first eigenfrequency is located at 185 Hz (Fig. 26 right).

With both FEMs, also a strength analysis was done consisting of a quasi-static, a sine, and a random response analysis against the mechanical S/C loads available at the time. For both the optical bench and the electronic box, in all analyses and for all axes, both in ultimate and in yield, margins of safety are positive in general. There are a few exceptions in random X response (optical bench), in the random Z response in the interconnections between PCBs and frames (electronic box) and against slippage of the fasteners (in optical bench and electronic box). These negative margins, if still existing after refinement of the S/C loads, can be easily solved by implementing small reinforcements in the design. As an example, Fig. 27 (left) gives the stresses in the warm base plate for quasi-static loading, and Fig. 27 (right) in one of the frames in the electronic box in random Y.

Structural modeling and analysis were performed by FHNW (Switzerland) for the optical bench and IDR-UPM (Spain) for the electronic box.

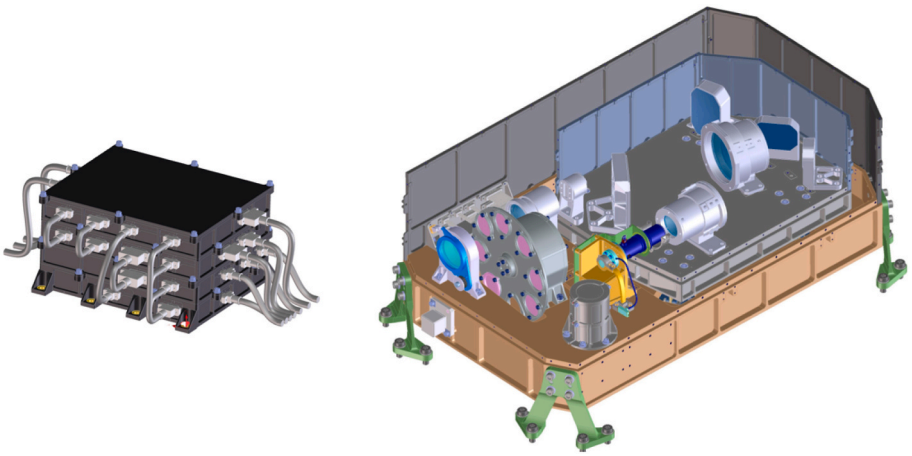

Fig. 22. 3D drawings of the electronic box (left) and the optical bench (right).

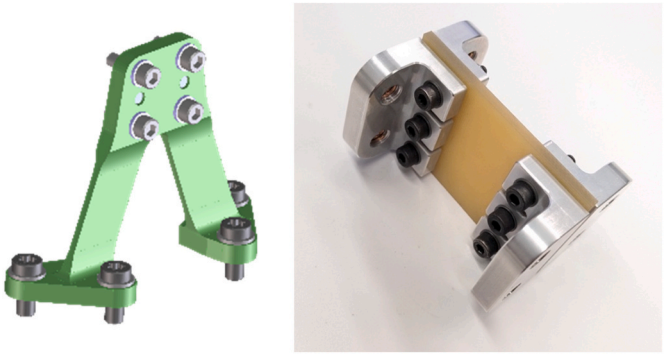

Fig. 23. Preliminary 3D drawing of the interface feet to the S/C (left) and picture of one of the flexures between cold and warm section (right).

10.3. Optical alignment

The internal alignment of the optical path will be performed while the instrument is operational, i.e., inside a vacuum chamber, with the cold section at −45 °C and the focal plane array cooled down to 120 K. Parts that need to be aligned are the illumination optics (one degree of freedom, linear along the optical axis) and the detector head (all six degrees of freedom).

The orientation of the LoS of VenSpec-H will be known with respect to an alignment cube, mounted externally on the nadir-face of the warm base plate. This cube will also be used during integration on the S/C for checking the misalignment with the spacecraft's mechanical axes. This misalignment is important when the pointing direction of the spacecraft must be calculated (needed when performing in-flight solar calibrations).

11. Thermal provisions and thermal modeling

11.1. Temperature management

VenSpec-H will be located completely inside a cavity of the EnVision S/C. It therefore is little subject to the extreme thermal conditions of the space environment. Only the instrument's aperture is logically exposed to space. The instrument is designed to look at Venus but can also safely look at the Sun for a certain duration (to perform solar calibrations).

VenSpec-H has three temperature reference points (TRP). TRP1 and TRP2 are indicated in Fig. 28. TRP1 is located at the thermal connection to the cold section (at the rear of the optical bench) and needs to be kept by the S/C at −45 °C ± 1 °C during operations. TRP1 is connected to a radiator via a thermal link managed by the S/C. TRP2 must be kept in a temperature range between −10 °C and 0 °C during operations. TRP2 is located at one of the lateral sides of the optical bench from where it is connected to a S/C radiator. The optical bench is thermally decoupled from the S/C by the titanium feet (conductive) and an outer multi-layer insulating blanket (MLI) (radiative). The cold section is thermally decoupled from the warm section by means of the four GFRP flexures (conductive) and an inner MLI (radiative). In Fig. 28 the thermal

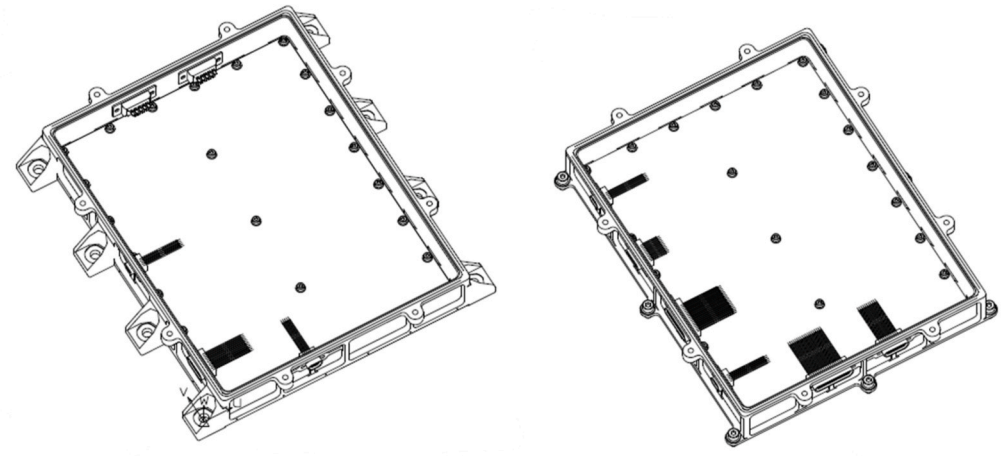

Fig. 24. Preliminary 3D drawing of the bottom frame (left) and one of the three upper frames (right) of the electronic box.

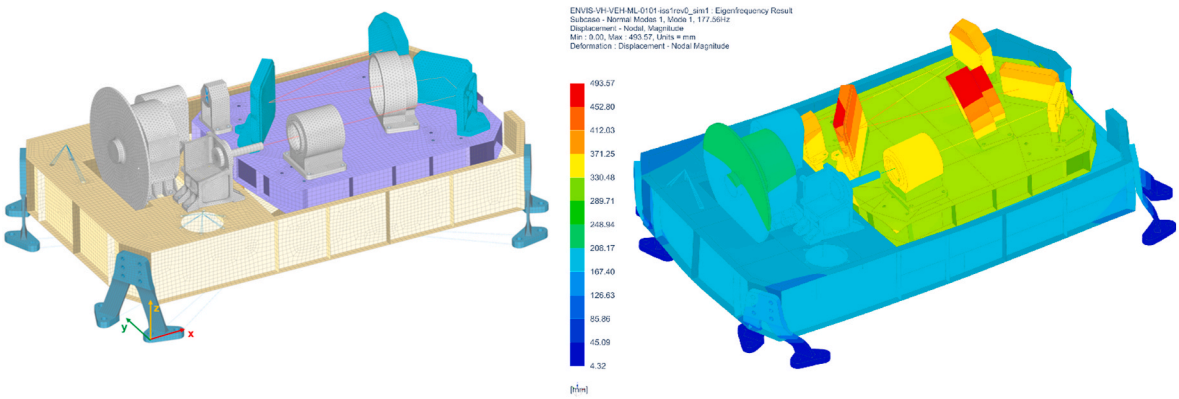

Fig. 25. FEM model of the optical bench (left) and first eigenmode (right).

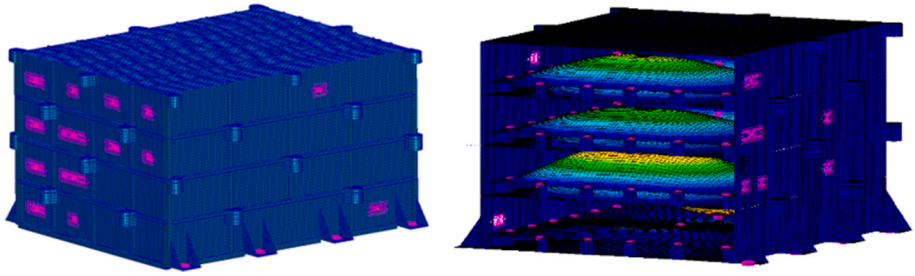

Fig. 26. FEM model of the electronic box (left) and first eigenmode (right).

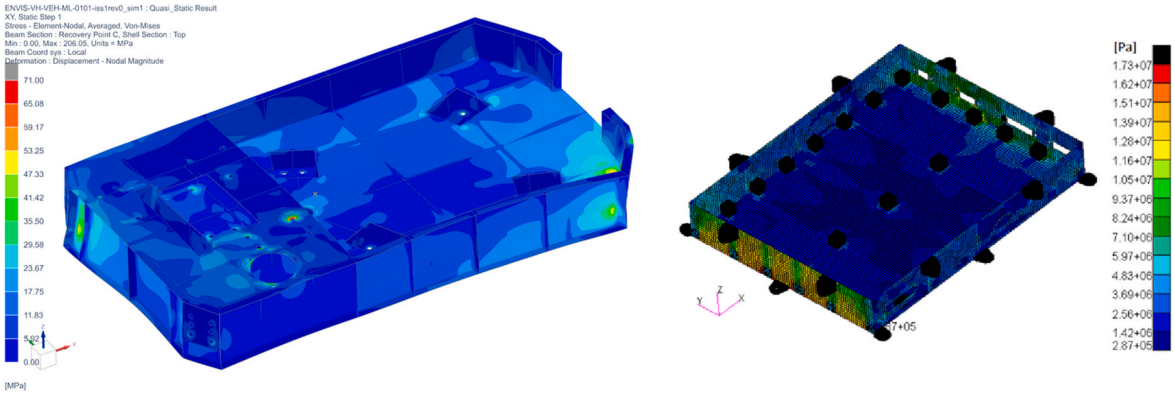

Fig. 27. Stresses in the warm base plate (quasi-static) (left) and in the FPGA frame of the electronic box (random Y) (right).

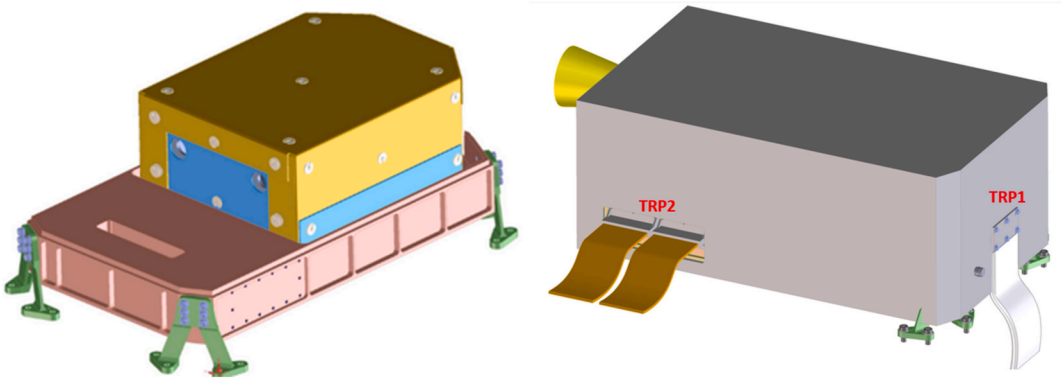

Fig. 28. Preliminary 3D drawing of cold section wrapped in two half MLI's (orange and blue) (left) and of warm section wrapped in MLI (grey) (right). (For interpretation of the references to colour in this figure legend, the reader is referred to the Web version of this article.)

connectors and the MLI concept are shown. Both the outer and inner MLI will have a twenty-layer lay-up including a Kapton black layer at the outside. The thermal blankets will consist of several individual pieces matching together and to the spacecraft MLI.

TRP3 is located at one of the feet of the electronic box. It will be kept between −30 °C and +45 °C by the S/C. The electronic box is thermally coupled to the S/C and carries no MLI.

When the instrument is not operating, TRP1 is guaranteed to be between −50 °C and +60 °C, TRP2 between −40 °C and +60 °C and TRP3 between −40 °C and +50 °C.

The detector's focal plane array and the cold shield in front are both located inside a vacuum dewar and connected to the tip of a cold finger (operating temperature is 120 K). A double linear compressor pumps heat from the cold finger and dumps it in the warm base plate of the optical bench.

On the warm part of the optical bench a chain of operational heaters will be installed. In case of low start-up temperature (below −30 °C) they allow to pre-heat the warm base plate so that filter wheel and detector can safely be activated. The warm base plate will also carry survival heaters, located close to the IDCA, that are commanded from the S/C. They will protect the IDCA in the unlikely case that the temperature of the warm section would drop below −40 °C during non-operation.

11.2. Thermal and geometrical mathematical model and analysis

Based on the CAD model of the instrument, a thermal and geometrical mathematical model (TGMM) was built in ESATAN, both for the optical bench and the electronic box. The TGMM has 980 nodes for the optical bench and 1′265 for the electronic box (Fig. 29).

For the optical bench, following thermal cases have been analyzed with the TGMM: hot operational steady state, hot and cold operational transient, hot and cold non-operational steady state, solar calibration and aerobraking. For the electronic box the most critical case is hot operational steady state. For all these cases temperature predictions have been made considering external contributors to the thermal behavior of VenSpec-H (e.g., radiative and conductive coupling with the S/C, light entering via the aperture, aerobraking flux, cooling by the radiators) and internal contributors (internal heat production, heat exchange between cold and warm section, heat exchange via harness between optical bench and electronic box).

The four S/C interface feet isolate the optical bench thermally from the S/C. Their thermal conductance is calculated to be 18.3 mW/K per foot in worst case. The four flexures that decouple the cold from the warm base plate each have a thermal conductance of 1.35 mW/K. The fixed pin between the two plates has a thermal conductance of 3 mW/K. The total thermal conductance between cold and warm section therefore is 8.4 mW/K.

VenSpec-H has a maximum power consumption of 61.3 W (including maturity and system margins), and hence dissipates a considerable amount of heat internally. Maximum power occurs during the ten first minutes of operation (so-called precooling phase) after which power consumption drops slightly to 50.3 W. Fig. 30 shows the analysis results for the most challenging hot operational transient case. The thermal gradient in the cold base plate is only 1.84 °C (requirement is 2 °C). The temporal stability over one dayside or nightside observation is 0.05 °C, much lower than the required 1 °C.

While the solar calibration case results in rather mild thermal conditions for the optical bench (the instrument is operational at that time and hence cooled), the aerobraking case seems to be the most demanding. The instrument is non-operational and can, in worst case, be thermally biased at +60 °C via the two radiators. Although the aperture of VenSpec-H will be nominally located at the anti-ram direction of the S/C during the dips in the atmosphere, in contingency situations the aerothermal flux could impact the aperture (at that time still closed by the shutter door), in worst case even combined with radiation from Venus or the Sun. Analysis results show rather high temperatures on the shutter mechanism (+68 °C on the body, +85 °C on the door support, +144 °C on the window). Besides the fact that a combination of such worst-case conditions is very unlikely, these temperatures are still low enough to not trigger the thermal knife that opens the door.

Most internal power will be dissipated inside the electronic box (38.3 W during precooling phase). This heat needs to be evacuated from the box even in the hot operational case where the S/C imposes an interface temperature of +45 °C. The thermal analysis of this case shows temperatures on some places in the printed circuit boards of +80 °C (Fig. 31) just at the limit of being acceptable.

Thermal modeling and analysis were performed by Space Acoustics (Switzerland) for the optical bench and IDR-UPM (Spain) for the electronic box.

11.3. Thermo-elastic analysis

The combined cold and warm optical bench has been designed to be insensitive against thermo-elastic deformations and, hence, to guarantee sufficient flatness and stability so that the performance of the optical path is not degraded. To verify this, thermo-elastic deformations were calculated with the FEM in all six degrees of freedom in a few optical points of interest (PoI) (Fig. 32). For this, a realistic thermal gradient map (both for hot and cold case) was included in the FEM. The resulting thermo-elastic deformation matrices were fed into the Code V optical model.

During this thermo-elastic study finetuning was done of the flexures between warm and cold base plate, and of the ribbing and shape of the base plates. Also, the spectrometer slit, the fixed pin and the focal plane array were put on one line, perpendicular to the optical axis. For the deformations to propagate as little as possible in the optical elements themselves, the optical holders will be made insensitive by means of kinematic mounts and dedicated lens barrel design. New iterations with the final optical holders will be performed in the future.

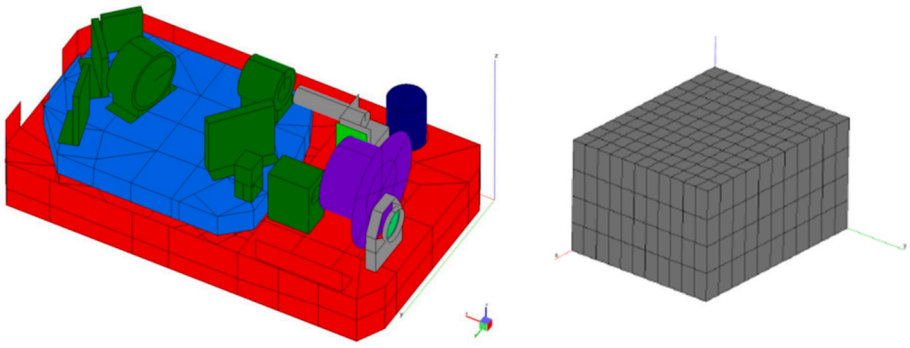

Fig. 29. Geometrical mathematical model of the optical bench (left) and electronic box (right).

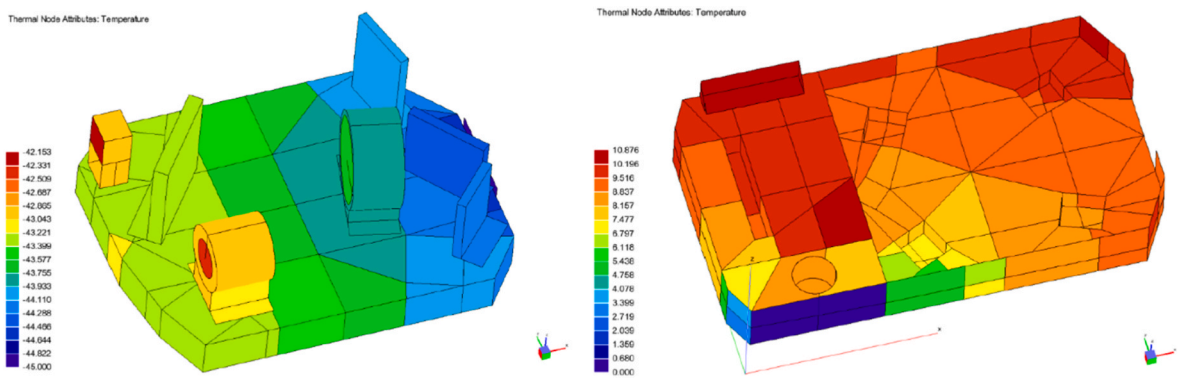

Fig. 30. Thermal analysis results hot operational case for the cold base plate (left) and the warm base plate (right).

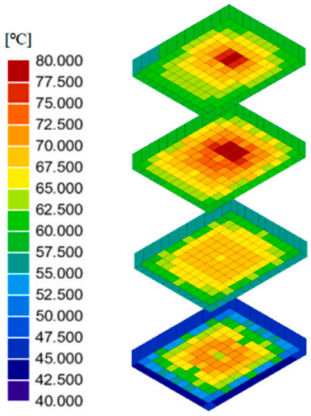

Fig. 31. Thermal analysis results hot operational steady state case for the electronic box.

12. Electronics, software and firmware design

12.1. Detector read-out and proximity electronics

In VenSpec-H a 384 × 288 pixels Mercury Cadmium Telluride (HgCdTe) (MCT) IDCA will be used. Each pixel of the detector is connected to a capacitance transimpedance amplifier (CTIA) with two integration capacitors (high and low gain). During a given integration time, the capacitors collect the electrons from the pixels via direct injection and store the charge. When integration is finished the charges are transferred into a sampling capacitor. The CTIA is reset, and a new integration period is started. During the next integration period the pixel charges of the previous cycle are converted to voltages and multiplexed into eight analog video signal outputs. The timing of the detector is autonomous and is synchronized to a master clock frequency. The detector can be programmed via SPI interface. Fig. 33 gives a block diagram of the ROIC. Two temperature sensing diodes are enclosed in the FPA for controlling the cooldown loop (typical operating temperature is 120 K). The detector signals exit via pins on the dewar. They form the electrical connection to the detector proximity electronics (via flex cable).

The detector proximity electronics (DEP) is a small printed circuit board (PCB) in close vicinity of the IDCA. It carries eight differential amplifiers that transform the single-ended analog output signals of the detector to differential signals (including buffering and level adaptation) and transmit them to the channel electronics in the detached electronic box.

12.2. Channel electronics

Except for the DEP-board, all other electronics boards will be physically located in a separate electronic box, completely detached from the optical bench.

The eight analog detector signals output from the IDCA are collected on the FPGA-board in differential amplifiers (identical to the ones on the

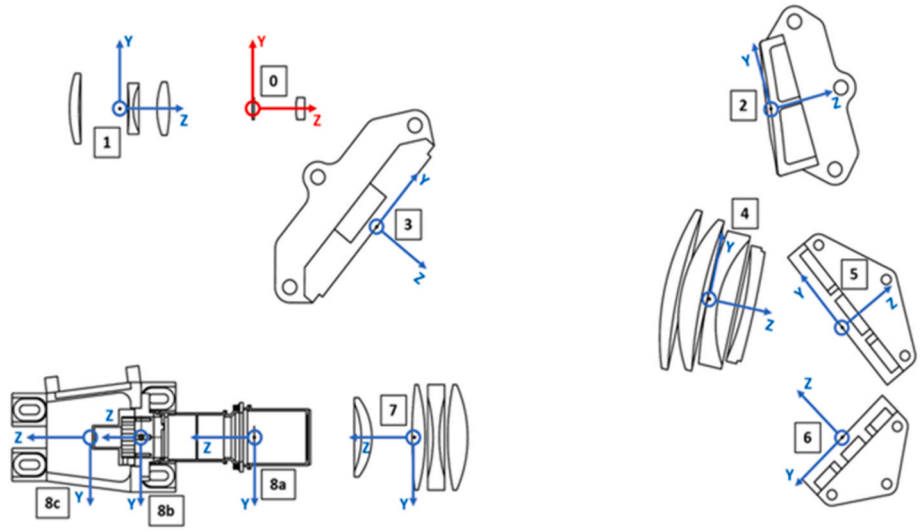

Fig. 32. Points of interest used during the thermo-elastic analysis (all cold PoI 44 mm above bench, all warm PoI 54 mm above bench).

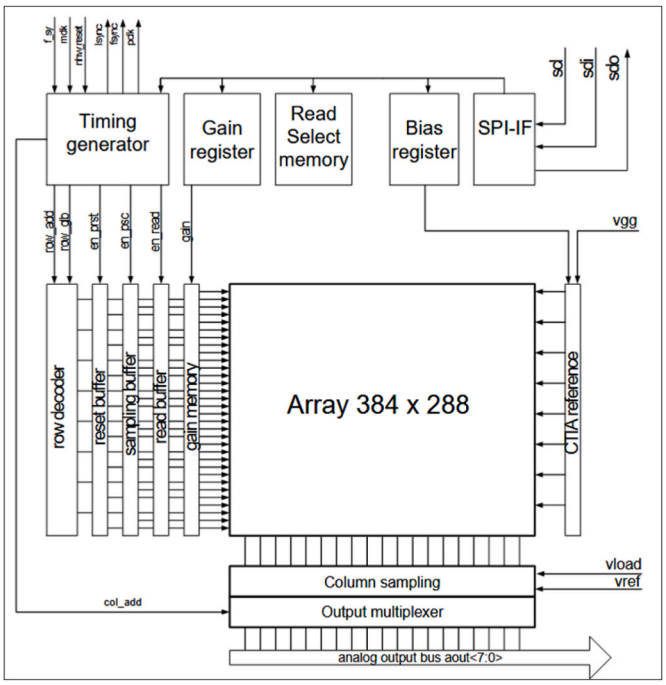

Fig. 33. Electronics block diagram of the detector ROIC (courtesy AIM).

DEP-board) and presented to eight analog-to-digital convertors (ran at 6.25 MHz to avoid a frequency notch imposed by one of the radars on board the S/C). The full read-out chain is shown in Fig. 34. The 14-bit wide digital output signals of the AD convertors are combined in two buses and clocked into an NX1H35AS NG-Medium field programmable gate array (FPGA) from NanoExplore.

Single detector frames will be temporarily stored in internal FPGA random-access memory where on-the-fly binning, accumulation, and background subtraction can be performed during measurements. This process runs at a clock frequency of 48 MHz and outputs 24-bit-wide values. As soon as a full detector frame is "treated" it will be either transmitted immediately to the processor board (PROC) over an internal SpaceWire link or transferred from internal FPGA memory to external static random-access memory (SRAM) on the FPGA board for later transmission. The FPGA acts also as a sequencer, executing all actions from the instrument timeline, i.e., sending control signals over LVDS to the motor driver board (MOD) for control of the cryocooler, the filter wheel, the shutter mechanism, the operational heaters, and for the collection of housekeeping data. Fig. 35 shows the layout of the FPGA-board. This is a prototype board where, unlike the flight version, the FPGA sits on an intermediate socket.

A combination of two full bridge drivers and four switching N-channel power MOSFETs, located on the MOD-board, will be used to drive the stepper motor of the filter wheel mechanism. Each phase of the motor is fed by a Pulse Width Modulated (PWM) signal generated in the FPGA. The FPGA uses micro-stepping to control the motor. For the dual compressor of the cryocooler this driver topology will be used as well. For the activation of the shutter mechanism and the operational heater chain, FETs switches are used to close a 24V power line and inject the appropriate current.

The central intelligence of the instrument is a SAMRH71 rad-hard microprocessor from Microchip Technologies located on the processor board (PROC). The controller is the interlink between the central Data Handling Unit (DHU) of the Venspec suite at one end, and the different subsystems of VenSpec-H at the other. It receives commands from the DHU (via SpaceWire), controls the mechanisms and the detector, gathers housekeeping, receives and temporarily stores science data frames, and transmits science and housekeeping frames to the DHU (via SpaceWire).

Peripheral to the processor are three magneto-resistive random-access memory devices (MRAM). One is configured as reprogrammable random-access memory and contains the bootloader of the system, and the running versions of the processor software and the FPGA bitstream. A second MRAM is configured as read-only volatile memory (EEPROM) and contains redundant fail-safe versions of bootloader, software and bitstream. The third MRAM is used as buffer for science data and housekeeping frames on their way to ground, or reversely, of uploaded patches for the processor and FPGA.

Several analog housekeeping parameters (currents, voltages, temperatures, position switches) are measured in the instrument, amplified, analog-to-digital converted and clocked into the processor once per second. Some of these parameters can be used in closed loop to control the subsystems, e.g., the Hall sensors of the shutter and filter wheel mechanisms, the temperature sensors of the detector (to regulate the cryocooler), and temperature sensors on the warm base plate (to control

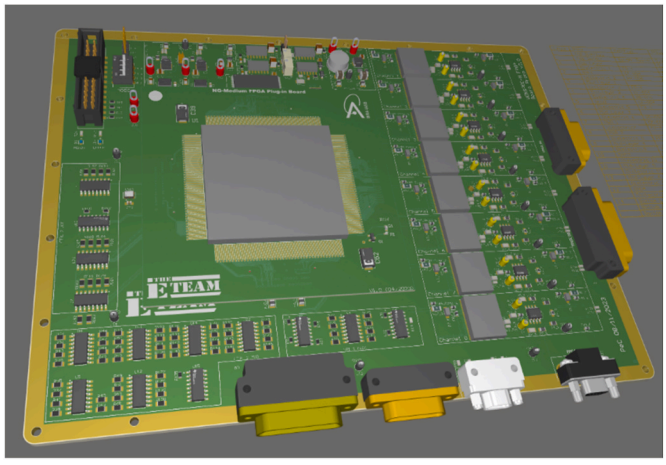

Fig. 35. Layout of the prototype FPGA-board.

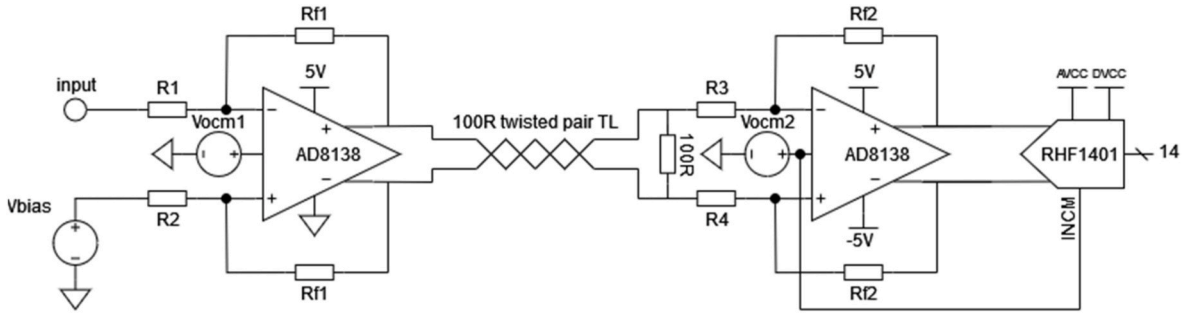

Fig. 34. Electronics scheme of the read-out chain of the detector.

the operational heater chain).

Fig. 36 gives a high-level block scheme of the VenSpec-H electronics.

12.3. Channel power supply unit

The electronic box houses a fourth PCB, the channel power supply unit (H-PSU) designed by IAA-CSIC (Spain) (Fig. 37). Two multi-output flyback converters with primary side control are the core of the power stage. These converters provide the isolation between the primary and secondary sides and generate the required secondary voltages.

The converters start up using a linear regulator fed from the filtered primary bus. As soon as they start, an auxiliary winding of the converters is used to power their controller circuit. One of these auxiliary voltages is used to supply the rest of the primary side circuits.

A +8V regulated voltage with floating ground, minimizing ground loops between power supply and detector, is produced for the detector proximity electronics (DEP board) and detector. The +3.3 V voltage has higher ripple, noise, and tolerance requirements and therefore this secondary output is regulated using a synchronous buck converter. Finally, also regulated +24V and ± 12V secondary outputs are foreseen.

The primary side circuits are protected against undervoltage to prevent the converters from starting before the required minimum voltage is reached. All secondary outputs are protected with over-current and over-voltage protection and passed through to the primary side via an optocoupler to disable the power supply and avoid permanent malfunction of the instrument. All protections (primary and secondary) are connected to a hiccup circuit that allows a controlled and safe reset of the power supply.

Output currents and voltages, as well as the temperature, are measured, A/D converted and transmitted to the PROC-board by SPI-bus.

12.4. On-board software and firmware

The on-board software, running in the microprocessor, is written in Python and C/C++. The FPGA runs a VHDL code. Both processor software and FPGA bitstream will reside in MRAM on the PROC-board. After switch-on, the processor will boot with nominal or redundant software and transfer the appropriate VHDL bitstream to the FPGA.

The processor runs a Real-Time Operating System (RTOS) from which the instrument timeline is executed. Fig. 38 shows a high-level block diagram of the on-board software. The following manager blocks can be distinguished: a telecommand manager (receiving telecommands from the S/C via the VenSpec DHU), a permanent memory manager (management of peripheral SRAM memory), an observation manager (preparing commands for the FPGA), a housekeeping manager (timing the collection of housekeeping data), a telemetry manager (preparing the data packets to be send to the S/C via the VenSpec DHU), a logging manager (composing a log register with all events), and a SpaceWire manager (controlling the internal and external SpaceWire links).

The FPGA code decodes commands, received from the processor, into hardware actions, such as generating signals for the cryocooler driver, placing the filter wheel in the requested position, programming the detector with the requested parameters, retrieving the analog data from the detector, performing binning, accumulation, and background subtraction, measuring local housekeeping, and transmitting data frames to the microprocessor. At the very start of the science part of the mission the FPGA will also open the shutter mechanism, and whenever needed, the operational heaters will be powered and controlled. Fig. 39 gives a block diagram of the code running in the FPGA.

12.5. Radiation analysis

The CAD file of the optical bench and the electronic box have been converted in a geometry description markup language (GDML) reduced model using the FASTRAD tool. Included in this model are a few well-chosen points-of-interest, materialized as box-like scoring volumes. To simulate shielding by the S/C, a hollow aluminium sphere is placed around the units. The sphere around the optical bench has an aperture corresponding to the aperture of the instrument (Fig. 40 left).

A total ionizing dose (TID) and total non-ionizing dose (TNID) radiation analysis have been performed for the scoring volumes using ESA's Geant4 radiation analysis for space (GRAS) tool. GRAS uses a general particle source (GPS) file, prepared in SPENVIS, as source generator for the primary particles, located on a sphere slightly larger than the sphere simulating the S/C (Fig. 40 right). For this study only long-term energetic particle spectra for solar energetic particles (SEP) (calculated with the SAPPHIRE total fluence model) and galactic cosmic rays (GCR) (calculated with the ISO-15390 model) have been considered, in accordance with the specified radiation environment for the EnVision mission.

The GRAS simulations were performed for 30 million (optical bench) resp. 10 million (electronic box) events (per run) to achieve adequate statistical accuracy in the results. For the scoring volumes in the electronic box TID is between 3.5 and 14.5 krad. At the FPA in the optical bench a TID of 4 krad is obtained. The TNID values are approximately $3.0 \times 10^{+8}$ MeV/g (electronic box) and $7.5 \times 10^{+7}$ MeV/g (detector).

Also, a preliminary short and long-term single event upset (SEU) analysis is performed with SPENVIS, using the CREME/CREME96

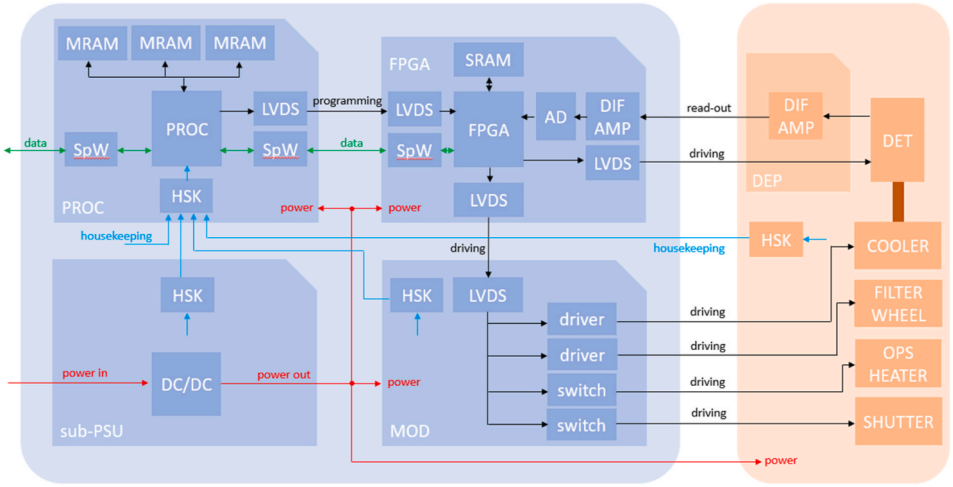

Fig. 36. Block diagram of electronics of VenSpec-H.

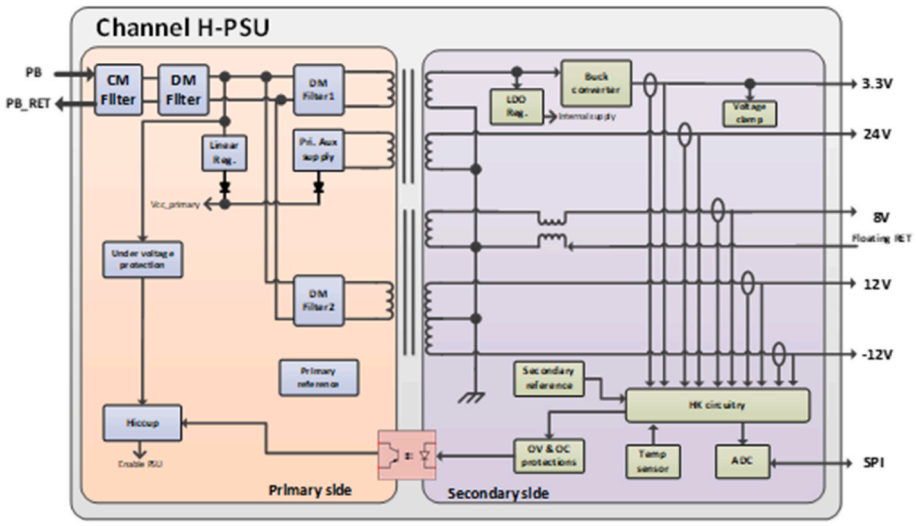

Fig. 37. H-PSU power distribution scheme.

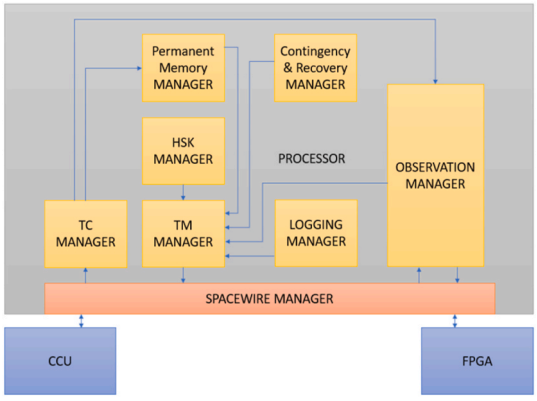

Fig. 38. VenSpec-H software block diagram.

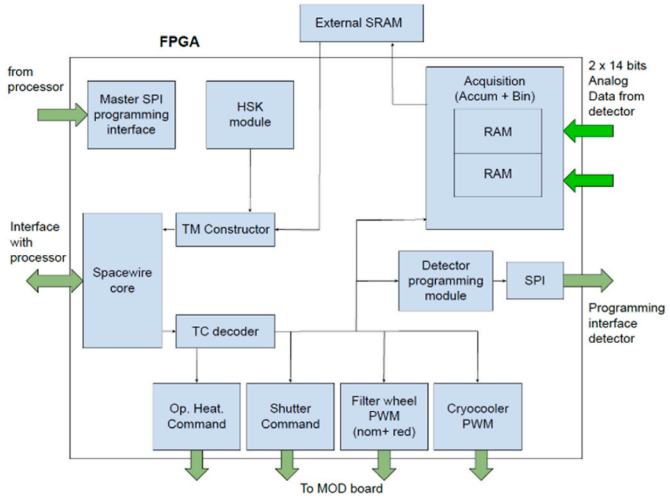

Fig. 39. VenSpec-H FPGA firmware block diagram.

method and the same omnidirectional particle spectrum radiation environment as for the total dose analysis. At the time of writing, the cross-sections, critical charge/LET thresholds, and sensitive volumes of the electronic devices under consideration were unknown. Therefore, a generic analysis was done for a discrete set of LET values in combination

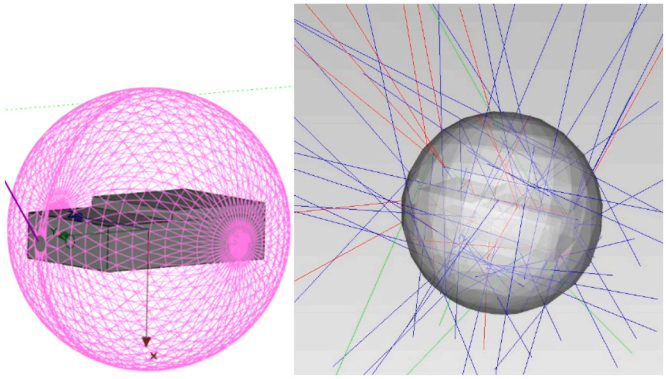

Fig. 40. Left: sphere around the optical bench simulating the S/C. Right: interaction of galactic cosmic rays protons (blue tracks) with the S/C shielding in GRAS Geant4 simulation. (For interpretation of the references to colour in this figure legend, the reader is referred to the Web version of this article.)

with arbitrarily chosen sensitive volume linear dimensions for direct ionization induced SEU rate.

These radiation analyses were performed by the SPENVIS team at BIRA-IASB (Belgium).

13. Observation sequence and modes

One orbit of the S/C around Venus takes approximately 5′640 s, meaning that there will be fifteen orbits per 24 h. The three VenSpec instruments will operate in a pure nadir mode and are active during four consecutive orbits out of the fifteen, i.e., an alternating suite of eight day and nightside sessions (Fig. 41). VenSpec-H will operate both at dayside (together with VenSpec-U) and at nightside (together with VenSpec-M). At the beginning of every observation (day or night) a new telecommand can be sent to the instrument programming it in the required scientific configuration.

From Fig. 41 it can be seen that VenSpec-H will be switched on well before the start of the observation sequence, i.e., already during the previous dayside or nightside. This is because the detector needs to be precooled for 600 s (precooling phase) to be operational when the science measurements start (science phase).

VenSpec-H has only three operating modes: “off”, “standby” and “observation”. This is depicted in Fig. 42. After switching on, the instrument will boot and go into standby, i.e., only the central electronics

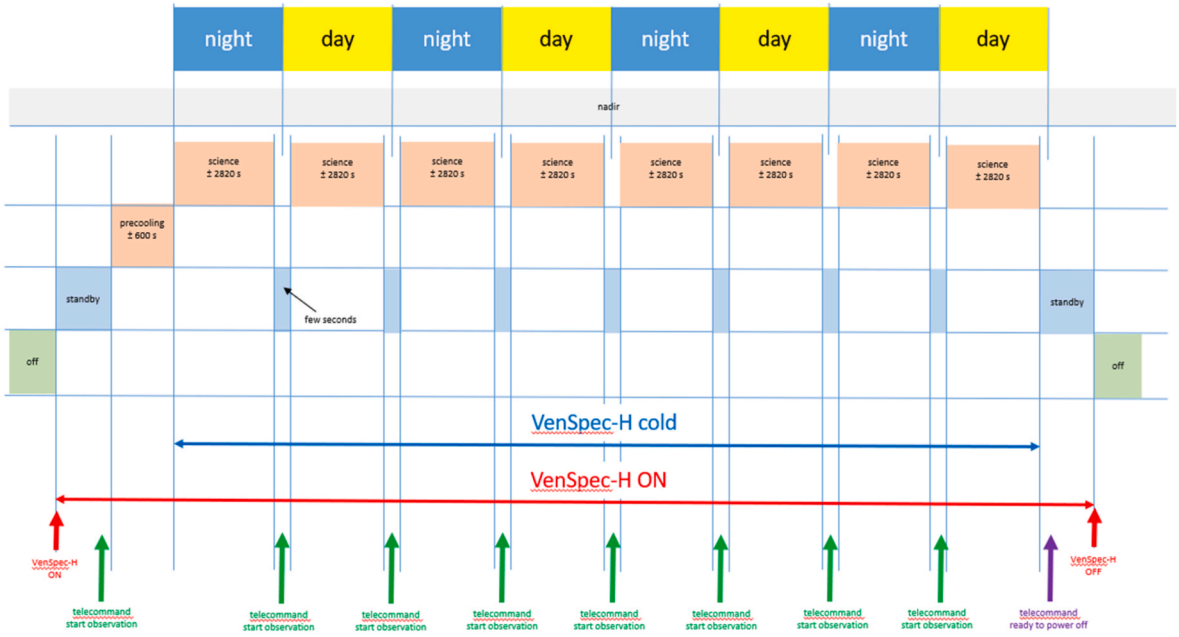

Fig. 41. VenSpec-H cyclogram with alternating sequence of 4 dayside and 4 nightside observations.

(processor and FPGA) are active and awaiting a command. Power consumption is minimal, no science data is produced, only small housekeeping frames every second.

Upon reception of a command from the CCU, the instrument will transition to observation mode. In this mode it will be first checked what the temperature is of the detector. If needed a precooling phase will be started to bring the detector down to its operating temperature (120 K). During precooling, power will be maximum because the cryocooler is running at full speed. Still no science data is produced, only larger housekeeping frames every second.

Once the detector is cooled, VenSpec-H will autonomously switch to the science phase and start recording spectra. Precooling will typically happen just prior to the first of the eight observations of a sequence. For the seven next observations the detector will be already cooled, and the science phase can start immediately after reception of a new command.

During the science phase the power consumption drops because the cryocooler throttles back from full power to regime mode, i.e., maintaining stable the operational temperature of the detector. Data rate increases dramatically in this phase. Besides the housekeeping frames, now also science frames are produced, on average 19.4 kbytes typically every second during dayside and every 15 s during nightside observations. At the end of an observation (a dayside or a nightside), the instrument will put itself back in standby mode, awaiting a new telecommand (new observation or switch-off).

Fig. 42 shows the power and data profiles for a typical observation with precooling at the start.

Each observation (either dayside or nightside) can be tailored to the scientific needs with a customized set of instrumental parameters.

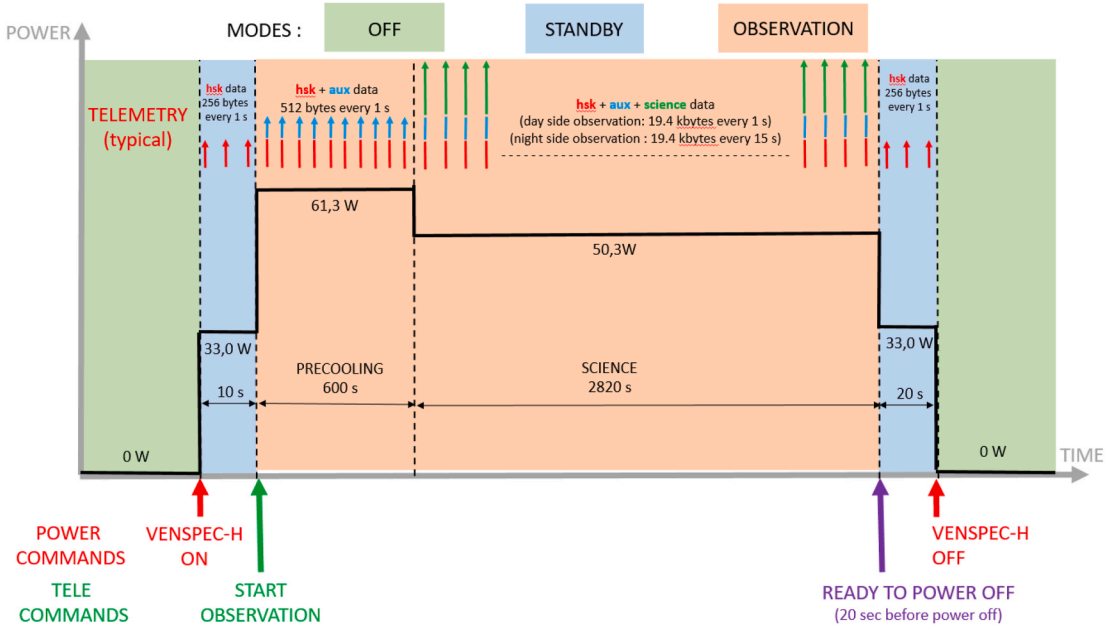

Fig. 42. Operational modes of VenSpec-H with corresponding power and data profiles.

Besides very basic technical settings, like the operational temperature of the detector or the angular velocity of the filter wheel, important parameters that can be programmed from ground are the integration time, the binning scheme, and the number of accumulations. Probably the most essential parameter is the filter wheel sequence that needs to be applied for each observation.

When signal is low, a series of consecutively registered spectra can be co-added pixel-by-pixel in on-board memory (accumulation) to increase the SNR. Also, spatial binning can be performed on-board. Here detector rows are co-added. In spectral band #2, binning is limited to the two horizontal filter zones #2a and #2b. In the other bands, binning over the full detector height is possible, considering however that there is always a part of the detector, corresponding to the blackened transition zone in the slit, that will not be used.

In-flight calibration sessions (solar and dark calibrations) follow the same operational pattern as the regular observations. In these sessions, full detector frames will be downlinked, without accumulation or binning. This results in a high data rate burst, which is acceptable since this type of observation will appear only every 112 days and will be planned when sufficient downlink capacity is available on the S/C.

One Sun calibration consists of six double S/C slews over the centre of the solar disk, one for each filter in the filter wheel (Fig. 43). These slews are called “double” because first a right-to-left passage over the Sun is performed pointing the centre of VenSpec-H’s bottom FoV (red cross), after which the S/C slewing is reversed and offset to pass over the centre of the top FoV (green cross).

The earlier mentioned APE/RPE requirements guarantee that during the very first calibration session, the centre of the solar disk passes through the FoV. The information from this first calibration session will be used to refine the pointing of the S/C for all subsequent observations and calibrations. The first solar calibration will be performed prior to the aerobraking phase of the mission, so that a perfect pointing law can be defined by the time the science phase of the mission starts.

Solar calibration is not only needed for LoS and FoV extent definition, and subsequent finetuning of the S/C pointing. Other in-flight calibration goals are to check the pixel-to-wavelength spectral calibration by means of the Fraunhofer lines in the solar spectrum, to radiometrically calibrate the instrument and check that the instrument performance is not degrading over time, and to determine the instrument sensitivity to linearly polarised light by looking at the solar disk with both unpolarised and linearly polarised filters.

14. Conclusions

The versatility of an echelle grating near-infrared spectrometer for the observation of planetary atmospheres has been proven by the tremendous successes of SOIR on Venus-Express (study of the Venus atmosphere) and the SO and LNO channels of NOMAD on ExoMars-TGO (study of the Martian atmosphere). While SOIR and NOMAD-SO were solar occultation instruments only, NOMAD-LNO offered additionally the possibility to perform nadir observations.

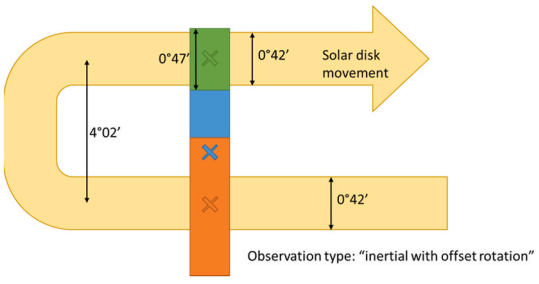

Fig. 43. Schematic representation of a double solar slew for one filter wheel position over the two filter sections (green and orange). (For interpretation of the references to colour in this figure legend, the reader is referred to the Web version of this article.)
Note 1: blue region denotes the non-illuminated zone of the detector.
Note 2: sizes of the sections not to scale.

VenSpec-H is completely dedicated to nadir observations, crucial to be able to probe also through the clouds at night and observe the lower layers of the Venusian atmosphere. For this purpose, where measuring in only a few spectral bands is aimed at, AOTF order sorting has been deemed unnecessary. Instead, an approach is adopted with dedicated filters. Cooling down the spectrometer section of VenSpec-H to −45 °C will lower thermal background, increase SNR, and, in general, improve significantly the scientific performance compared to NOMAD-LNO.

Although VenSpec-H builds on quite some heritage from its predecessors, parts of the instrument are new. Running an instrument with an optical bench that consists of two base plates at different temperatures is challenging. Having optical elements, like grating, filter-slit-assembly, parabolic mirror, and freeform corrector plate well aligned and perform accurately at low temperature, needed careful design.

In this article an overview was given of the design work for VenSpec-H and it is shown that an instrument can be build fulfilling the science requirements and the EnVision mission requirements. Additionally, modeling and a series of analysis efforts have given confidence that the instrument will survive the environmental conditions on its journey to and stay in the vicinity of Venus.

Building and physically testing the instrument is now the next step. It goes without saying that also during manufacturing, assembly, integration and testing, many challenges will have to be faced. Yet, a better starting point than the solid design that is presented here, is not possible. No real blocking points are identified so far and, hence, a timely delivery of the flight model of the instrument to ESA and the S/C Prime in 2029 is anticipated.

CRediT authorship contribution statement

E. Neefs: Conceptualization, Project administration, Supervision, Writing – original draft, Writing – review & editing. **A.C. Vandaele:** Investigation. **R. De Cock:** Investigation. **J. Erwin:** Investigation, Project administration. **S. Robert:** Investigation, Supervision. **I.R. Thomas:** Investigation. **S. Berkenbosch:** Investigation. **L. Jacobs:** Investigation. **P. Bogaert:** Investigation. **B. Beeckman:** Investigation. **A. Brassine:** Investigation. **N. Messios:** Investigation. **E. De Donder:** Investigation. **D. Bolsée:** Investigation. **N. Pereira:** Investigation. **P. Tackley:** Investigation. **T. Gerya:** Investigation. **S. Kögl:** Investigation. **P. Kögl:** Investigation. **H.-P. Gröbelbauer:** Conceptualization. **F. Wirz:** Investigation. **G. Székely:** Investigation. **N. Eaton:** Investigation. **E. Roibás-Millán:** Investigation. **I. Torralbo:** Investigation. **H. Rubio-Arnaldo:** Investigation. **J.M. Alvarez:** Investigation. **D. Navajas Ortega:** Investigation. **L. De Vos:** Investigation. **R. Sørensen:** Investigation. **W. Moelans:** Investigation. **A. Algoedt:** Investigation. **M. Blau:** Investigation. **D. Stam:** Investigation. **E. Renotte:** Investigation, Investigation. **P. Klinkenberg:** Investigation. **B. Borguet:** Investigation. **S. Thomas:** Investigation. **M. Vervaeke:** Investigation. **H. Thienpont:** Investigation. **J.M. Castro:** Investigation. **J. Jimenez:** Investigation.

Declaration of competing interest

The authors declare that they have no known competing financial interests or personal relationships that could have appeared to influence the work reported in this paper.

Acknowledgements

The VenSpec-H instrument design, modeling and analysis has been performed under the responsibility of a Belgian Instrument Lead team (BIRA-IASB, Brussels). Warm thanks go to the scientists of the Planetary Atmospheres division and the engineers and technicians of the Engineering Department at BIRA-IASB. We also thank all associated science

and engineering teams, linked to research institutes or industrial companies in Europe, that contributed to this work:

•in Switzerland: ETHZ, KOEGL Space, FHNW, HSLU, and Space Acoustics.

•in Spain: IDR-UPM and IAA-CSIC.

•in The Netherlands: Leiden Observatory.

•in Germany: DLR and AIM.

•in Belgium: OIP, AMOS and B-PHOT VUB.

We are grateful to ESA for giving the science community the chance to go to Venus (again). Our special thanks to the EnVision project team and the PRODEX team at ESTEC that follow the design of VenSpec-H attentively.

The Belgian and Swiss work described in this article has been made possible thanks to funding by the Belgian Science Policy Office (BELSPO) (Prodex Experiment Agreement 4000128137), the Swiss Space office (SSO) (Prodex Experiment Agreements 4000138690, 4000138246 and 4000138247) and financial and contractual coordination by the ESA Prodex Office. The Spanish contribution has been supported by the Agencia Estatal de Investigación under grants PID2021-126365NB-C21 and PID2021-126365NA-C22.

References

[1] D. Nevejans, E. Neefs, E. Van Ransbeeck, S. Berkenbosch, R. Clairquin, L. De Vos, W. Moelans, S. Glorieux, A. Baeke, O. Korablev, I. Vinogradov, Y. Kalinnikov, B. Bach, J.-P. Dubois, E. Villard, Compact high-resolution spaceborne echelle grating spectrometer with acousto-optical tunable filter based order sorting for the infrared domain from 2.2 to 4.3 μm, Appl. Opt. 45 (21) (2006) 5191–5206, https://doi.org/10.1364/AO.45.005191.

[2] A. Mahieux, A.C. Vandaele, S. Robert, V. Wilquet, R. Drummond, F. Montmessin, J. L. Bertaux, Densities and temperatures in the Venus mesosphere and lower thermosphere retrieved from SOIR on board Venus Express: carbon dioxide measurements at the Venus terminator, J. Geophys. Res. 117 (2012) E07001, https://doi.org/10.1029/2012JE004058.

[3] V. Wilquet, R. Drummond, A. Mahieux, S. Robert, A.C. Vandaele, J.L. Bertaux, Optical extinction due to aerosols in the upper haze of Venus: four years of SOIR/VEX observations from 2006 to 2010, Icarus 217 (2) (2012) 875–881, https://doi.org/10.1016/j.icarus.2011.11.002.

[4] A.C. Vandaele, A. Mahieux, S. Robert, R. Drummond, V. Wilquet, J.-L. Bertaux, Carbon monoxide short term variability observed on Venus with SOIR/VEX, Planet. Space Sci. 113–114 (2014) 237–255, https://doi.org/10.1016/j.pss.2014.12.012.

[5] O. Korablev, J.-L. Bertaux, D. Nevejans, the SOIR instrument team, Compact high resolution IR spectrometer for atmospheric studies, Geophys. Res. Abstr. 5 (2003) 14785.

[6] O.I. Korablev, J.-L. Bertaux, I.I. Vinogradov, Y.K. Kalinnikov, D. Nevejans, E. Neefs, T. Le Barbu, G. Durry, Compact high-resolution echelle–AOTF NIR spectrometer for atmospheric measurements, in: B. Warmbein (Ed.), Proceedings of the 5th International Conference on Space Optics (ICSO 2004), ESA Spec. Publ. SP-554, 2004, pp. 73–80.

[7] O. Korablev, J.-L. Bertaux, I.I. Vinogradov, Y.K. Kalinnikov, D. Nevejans, E. Neefs, T. Le Barbu, G. Durry, A. Fedorova, A. Grigoriev, High resolution spectrometers for planetary spacecraft, in: Presented at the 35th COSPAR Scientific Assembly, 18–25 July 2004. Paris, France.

[8] E. Neefs, A.C. Vandaele, R. Drummond, I. Thomas, S. Berkenbosch, R. Clairquin, S. Delanoye, B. Ristic, J. Maes, S. Bonnewijn, G. Pieck, E. Equeter, C. Depiesse, F. Daerden, E. Van Ransbeeck, D. Nevejans, J. Rodriguez, J.-J. Lopez-Moreno, R. Sanz, R. Morales, G.P. Candini, C. Pastor, B. Aparicio del Moral, J.-M. Jeronimo, J. Gomez, I. Perez, F. Navarro, J. Cubas, G. Alonso, A. Gomez, T. Thibert, M. Patel, G. Belucci, L. De Vos, S. Lesschaeve, N. Van Vooren, W. Moelans, L. Aballea, S. Glorieux, A. Baeke, D. Kendall, J. De Neef, A. Soenen, P.-Y. Puech, J. Ward, J.-F. Jamoye, D. Diez, A. Vicario, M. Jankowski, NOMAD spectrometer on the ExoMars trace gas orbiter mission: part 1—design, manufacturing and testing of the infrared channels, Appl. Opt. 54 (28) (2015) 8494–8520, https://doi.org/10.1364/AO.54.008494.

[9] A.C. Vandaele, J.-J. Lopez-Moreno, M. Patel, G. Bellucci, F. Daerden, B. Ristic, S. Robert, I. Thomas, V. Wilquet, M. Allen, G. Alonso-Rodrigo, F. Altieri, S. Aoki, D. Bolsée, T. Clancy, E. Cloutis, C. Depiesse, R. Drummond, A. Fedorova, V. Formisano, B. Funke, F. González-Galindo, A. Geminale, J.-C. Gérard, M. Giuranna, L. Hetey, N. Ignatiev, J. Kaminski, O. Karatekin, Y. Kasaba, M. Leese, F. Lefèvre, S. Lewis, M. López-Puertas, M. López-Valverde, A. Mahieux, J. Mason, J. McConnell, M. Mumma, L. Neary, E. Neefs, E. Renotte, J. Rodriguez-Gomez, G. Sindoni, M. Smith, A. Stiepen, A. Trokhimovsky, J. Vander Auwera, G. Villanueva, S. Viscardy, J. Whiteway, Y. Willame, M. Wolff, M and the NOMAD Team, NOMAD, an integrated suite of three spectrometers for the ExoMars trace gas mission: technical description, science objectives and expected performance, Space Sci. Rev. 214 (5) (2018) A80, https://doi.org/10.1007/s11214-018-0517-2.

[10] O. Korablev, A.C. Vandaele, F. Montmessin, A. Fedorova, A. Trokhimovskiy, F. Forget, F. Lefèvre, F. Daerden, I. Thomas, L. Trompet, J. Erwin, S. Aoki, S. Robert, L. Neary, S. Viscardy, A. Grigoriev, N. Ignatiev, A. Shakun, A. Patrakeev, D. Belyaev, J.-L. Bertaux, K. Olsen, L. Baggio, J. Alday, Y. Ivanov, B. Ristic, J. Mason, Y. Willame, C. Depiesse, L. Hetey, S. Berkenbosch, R. Clairquin, C. Queirolo, B. Beeckman, E. Neefs, M. Patel, G. Bellucci, J.-J. López-Moreno, C. Wilson, G. Etiope, L. Zelenyi, H. Svedhem, J.L. Vago, the ACS and NOMAD science teams, No detection of methane on Mars from early ExoMars trace gas orbiter observations, Nature 568 (2019) 517–520, https://doi.org/10.1038/s41586-019-1096-4.

[11] G. Liuzzi, G. Villanueva, M. Mumma, M. Smith, F. Daerden, B. Ristic, I. Thomas, A. C. Vandaele, M. Patel, J.-J. Lopez-Moreno, G. Bellucci, Methane on Mars: new insights into the sensitivity of CH4 with the NOMAD/ExoMars spectrometer through its first in-flight calibration, Icarus 321 (11) (2019) 670–691, https://doi.org/10.1016/j.icarus.2018.09.021.

[12] A.C. Vandaele, O. Korablev, F. Daerden, S. Aoki, I. Thomas, F. Altieri, M. López-Valverde, G. Villanueva, G. Liuzzi, M. Smith, J. Erwin, L. Trompet, A. Fedorova, F. Montmessin, A. Trokhimovskiy, D. Belyaev, N. Ignatiev, M. Luginin, K. Olsen, L. Baggio, J. Alday, J.-L. Bertaux, D. Betsis, D. Bolsée, T. Clancy, E. Cloutis, C. Depiesse, B. Funke, M. Garcia-Comas, J.-C. Gérard, M. Giuranna, F. Gonzalez-Galindo, A. Grigoriev, Y. Ivanov, J. Kaminski, O. Karatekin, F. Lefèvre, S. Lewis, M. López-Puertas, A. Mahieux, I. Maslov, J. Mason, M. Mumma, L. Neary, E. Neefs, A. Patrakeev, D. Patsaev, B. Ristic, S. Robert, F. Schmidt, A. Shakun, N. Teanby, S. Viscardy, Y. Willame, J. Whiteway, V. Wilquet, M. Wolff, G. Bellucci, M. Patel, J.-J. López-Moreno, F. Forget, C. Wilson, H. Svedhem, J. Vago, D. Rodionov, the NOMAD and ACS science teams, Martian dust storm impact on atmospheric H2O and D/H observed by ExoMars Trace Gas Orbiter, Nature 568 (2019) 521–525, https://doi.org/10.1038/s41586-019-1097-3.

[13] P. Drossart, G. Piccioni, A. Adriani, F. Angrilli, G. Arnold, K. Baines, G. Bellucci, J. Benkhoff, B. Bézard, J.-P. Bibring, A. Blanco, M. Blecka, R. Carlson, A. Coradini, A. Di Lellis, T. Encrenaz, S. Erard, S. Fonti, V. Formisano, T. Fouchet, R. Garcia, R. Haus, J. Helbert, N. Ignatiev, P. Irwin, Y. Langevin, S. Lebonnois, M. Lopez-Valverde, D. Luz, L. Marinangeli, V. Orofino, A. Rodin, M. Roos-Serote, B. Saggin, A. Sanchez-Lavega, D. Stam, F. Taylor, D. Titov, G. Visconti, M. Zambelli, R. Hueso, C. Tsang, C. Wilson, T. Afanasenko, Scientific goals for the observation of Venus by VIRTIS on ESA/Venus Express mission, Planet. Space Sci. 55 (2007) 1653–1672, https://doi.org/10.1016/j.pss.2007.01.003.

[14] G. Piccioni, P. Drossart, E. Suetta, M. Cosi, E. Amannito, A. Barbis, R. Berlin, A. Bocaccini, G. Bonello, M. Bouyé, et al., VIRTIS: the visible and infrared thermal imaging spectrometer, ESA Spec. Publ. (2007) 1–27, 2007, SP 1295.

[15] EnVision. Understanding why our most Earth-like neighbour is so different, ESA M5 proposal 1-43 (2016) 2016.

[16] EnVision. Understanding why our most Earth-like neighbour is so different, EnVision Assessment Study Report (Yellow Book), ESA/SCI 1 (2021), 2021.

[17] J. Helbert, A.-C. Vandaele, E. Marcq, S. Robert, C. Ryan, G. Guignan, Y. Rosas-Ortiz, E. Neefs, I.R. Thomas, G. Arnold, G. Peter, T. Widemann, L. Lara, The VenSpec suite on the ESA EnVision mission to Venus, in: Proceedings of SPIE 11128: Infrared Remote Sensing and Instrumentation XXVII, 9 September 2019, https://doi.org/10.1117/12.2529248. San Diego, USA.

[18] J. Helbert, M. Dyar, I. Walter, D. Wendler, T. Widemann, E. Marcq, G. Guignan, S. Ferrari, A. Maturilli, N. Mueller, D. Kappel, et al., The Venus emissivity mapper (VEM): obtaining global mineralogy of Venus from orbit, Infrared Remote Sensing and Instrumentation XXVI (August 2018), https://doi.org/10.1117/12.2320112). San Diego, United States. pp.art. 107650D.

[19] E. Marcq, G. Guignan, B. Lustrement, F. Montmessin, J. Lasue, B. Bézard, A.-C. Vandaele, J. Helbert, T. Widemann, C. Wilson, R. Ghail, et al., Monitoring Venus cloud top: the VenSpec-U spectrometer on board ESA EnVision, Europlanet Science Congress 14 (2020) EPSC2020–E2622, https://doi.org/10.5194/epsc2020-622. September 2020, Germany.

[20] J. Vanhamel, A.C. Vandaele, E. Neefs, S. Robert, L. Jacobs, S. Berkenbosch, I. Thomas, B. Beeckman, W. Moelans, S. Lesschaeve, A. Algoedt, L. De Vos, M. Vaughan, Design and development of the VenSpec-H instrument, Euro Planets Sciene Congress 14 (2020) EPSC2020–E2535, https://doi.org/10.5194/epsc2020-535, 2020.

[21] R. DeCock, A.C. Vandaele, E. Neefs, J. Erwin, S. Robert, I. Thomas, S. Berkenbosch, L. Jacobs, P. Bogaert, B. Beeckman, A. Brassine, E. De Donder, N. Messios, P. Tackley, T. Gerya, S. Kögl, G. Székely, H.-P. Gröbelbauer, F. Wirz, N. Eaton, E. Roibás-Millán, I. Torralbo, H. Rubio-Arnaldo, J.M. Álvarez, D. Navajas-Ortega, R. Sørensen, L. De Vos, M. Blau, W. Moelans, A. Algoedt, D. Stam, the VenSpec-H team, VenSpec-H: high-resolution IR spectrometer on ESA's EnVision mission to Venus, in: 2023 International EnVision Venus Science Workshop, 9 - 11 May 2023, 2023. Berlin, Germany.

[22] E. Roberts, M. Eiden, A Space Tribology Handbook, 1998 corpus ID: 137357088.

[23] H. Höhnemann, S. Hanna, A. Sieck, R. Thöt, M. Benecke, J. Wendler, A. Weber, D. Hübner, H. Figgemeier, R. Breiter, W. Gross, VIS/SWIR IR detectors for space applications at AIM: models and qualification status, in: Proceedings Volume 11180, International Conference on Space Optics — ICSO 2018, 2019 111803F, https://doi.org/10.1117/12.2536042.